

# Geochemistry, Geophysics, Geosystems®

## RESEARCH ARTICLE

10.1029/2024GC011869

### Key Points:

- Two radiogenic isotope endmembers are identified: the Karoo and Cape Supergroup provenance types
- The spatial variability of clay mineral abundances in the river sediments can be explained by changes in chemical weathering intensity
- Accurately interpreting sediment provenance is essential for paleoclimatic reconstructions using marine sediment cores

### Supporting Information:

Supporting Information may be found in the online version of this article.

### Correspondence to:

E. J. Pryor,  
[ellie.pryor@uib.no](mailto:ellie.pryor@uib.no)

### Citation:

Pryor, E. J., Hall, I. R., Simon, M. H., Andersen, M., Babin, D., Starr, A., et al. (2025). Geochemical—mineralogical constraints on the provenance of sediment supplied from South African river catchments draining into the southwestern Indian Ocean. *Geochemistry, Geophysics, Geosystems*, 26, e2024GC011869. <https://doi.org/10.1029/2024GC011869>

Received 10 SEP 2024

Accepted 8 APR 2025

### Author Contributions:

**Conceptualization:** E. J. Pryor, I. R. Hall, M. H. Simon, A. Starr, H. J. L. van der Lubbe

**Data curation:** E. J. Pryor, I. R. Hall, D. Babin, A. Starr, H. J. L. van der Lubbe

**Funding acquisition:** E. J. Pryor, M. H. Simon






**Investigation:** E. J. Pryor, I. R. Hall, D. Babin, A. Lipp, H. J. L. van der Lubbe

**Methodology:** E. J. Pryor, M. Andersen, A. Starr, H. J. L. van der Lubbe

**Supervision:** I. R. Hall, M. H. Simon, M. Andersen, H. J. L. van der Lubbe

© 2025 The Author(s). Geochemistry, Geophysics, Geosystems published by Wiley Periodicals LLC on behalf of American Geophysical Union. This is an open access article under the terms of the [Creative Commons Attribution License](#), which permits use, distribution and reproduction in any medium, provided the original work is properly cited.

## Geochemical—Mineralogical Constraints on the Provenance of Sediment Supplied From South African River Catchments Draining Into the Southwestern Indian Ocean

E. J. Pryor<sup>1,2</sup> , I. R. Hall<sup>1</sup> , M. H. Simon<sup>3,4</sup>, M. Andersen<sup>1</sup>, D. Babin<sup>5</sup> , A. Starr<sup>6</sup> , A. Lipp<sup>7</sup>, and H. J. L. van der Lubbe<sup>8</sup> 

<sup>1</sup>Cardiff University, School of Earth and Environmental Sciences, Cardiff, UK, <sup>2</sup>Now at Department of Earth Sciences, University of Bergen, Norway; SFF Centre for Early Sapiens Behaviour (SapienCE), Bergen, Norway, <sup>3</sup>NORCE Norwegian Research Centre, Bjerknes Centre for Climate Research, Bergen, Norway, <sup>4</sup>SFF Centre for Early Sapiens Behaviour (Sapien CE), Bergen, Norway, <sup>5</sup>Lamont-Doherty Earth Observatory of Columbia University, New York, NY, USA, <sup>6</sup>Department of Geography, University of Cambridge, Cambridge, UK, <sup>7</sup>Department of Earth Sciences, University College London, London, UK, <sup>8</sup>Department of Earth Sciences, Cluster Geochemistry & Geology, Vrije Universiteit Amsterdam (VU), Amsterdam, The Netherlands

**Abstract** This study utilizes the radiogenic isotopes of neodymium (Nd) and strontium (Sr) measured in river mud—which serves as a proxy for the suspended load—to examine how source-rock lithology and weathering intensity impact the composition of material delivered to marine sediments along the Southeast African continental margin. Sediments were sampled from 22 river catchments between Durban and Cape Town in South Africa. Two distinct endmembers (i.e., geographical source areas) characterizing the regional river systems were identified. According to endmember modeling, rivers of the Eastern Cape drain soils weathered of the Karoo Supergroup and Drakensberg basalts ( $^{87}\text{Sr}/^{86}\text{Sr}$  of 0.74049 and  $\epsilon\text{Nd}$  of  $-8.53$ ), whereas rivers of the Southern Cape drain the Cape Supergroup, exhibiting more radiogenic  $^{87}\text{Sr}/^{86}\text{Sr}$  ratios (0.74596) and unradiogenic  $\epsilon\text{Nd}$  values ( $-10.09$ ). River sediments from the Karoo Supergroup are finer-grained compared to those from the Cape Supergroup. We analyzed clay mineralogy and two grain size fractions ( $<2\ \mu\text{m}$ ;  $2\text{--}32\ \mu\text{m}$ ) from co-registered samples, and the results suggest that the spatial variability in the  $^{87}\text{Sr}/^{86}\text{Sr}$  values is due to the lower degree of chemical weathering of silicate rocks and increased illite abundances toward the south, which a simple mixing model can explain. Kaolinite abundance decreased from Northeast to Southwest within South African coastal river catchments. In contrast, illite abundances increased due to diminished chemical weathering in the southern regions driven by the weaker rainfall regime. As demonstrated in this study, combining geochemical tools provides a reliable foundation for provenance studies of offshore marine sediment studies.

**Plain Language Summary** Radiogenic isotopes are measured in South African river muds to understand how the source rocks and weathering intensity influence sediments, which drain toward the Southwest Indian Ocean. 22 samples were collected from rivers between Durban and Cape Town in South Africa. Rivers from the Eastern Cape mostly carry sediments from the Karoo Supergroup and Drakensberg basalts ( $^{87}\text{Sr}/^{86}\text{Sr}$  of 0.74049 and  $\epsilon\text{Nd}$  of  $-8.53$ ), whereas rivers in the Southern Cape carry sediments from the Cape Supergroup ( $^{87}\text{Sr}/^{86}\text{Sr}$  of 0.74596 and  $\epsilon\text{Nd}$  of  $-10.09$ ), explained with a simple endmember mixing model. River sediments from the Karoo Supergroup are finer-grained than those from the Cape Supergroup. We analyzed clay mineralogy and two grain size fractions for  $^{87}\text{Sr}/^{86}\text{Sr}$  ( $<2\ \mu\text{m}$ ;  $2\text{--}32\ \mu\text{m}$ ) from co-registered samples. The geochemical composition of these sediments is related to the source rock and the degree of chemical weathering, the latter of which varies due to differences in rainfall regimes. In the Southern Cape region, which experiences less rainfall than the Eastern Cape, sediments contain more illite due to reduced chemical weathering. Finally, this study furthers our understanding of the use of geochemical tools for provenance work, which is essential for past climate studies using marine sediment cores.

## 1. Introduction

A substantial amount of sediment is deposited by rivers on continental margins and in the deeper parts of marine basins. As a result, marine sediment cores provide a long-lasting continuous archive of ocean and climate conditions in the past, and offer valuable insights into terrestrial climate changes, hydroclimate patterns and river discharge into the ocean. Past climate conditions can be inferred through proxy reconstructions by analyzing

**Writing – original draft:** E. J. Pryor  
**Writing – review & editing:** E. J. Pryor,  
I. R. Hall, M. H. Simon, M. Andersen,  
A. Lipp, H. J. L. van der Lubbe

geochemical signals recorded in the detrital minerals and fossil material. These signals can be correlated with climate or environmental parameters in the modern world (e.g., differences in geochemical elemental ratios or relative abundances of species can be interpreted as a change in climate conditions). Similarly, the provenance of detrital sediments (e.g., determination of geographical source areas of lithogenic sediments) can also indicate past environmental and climate conditions. Understanding erosion and pedogenic processes in the terrestrial source regions and transport pathways by which the sediment arrives at a marine sediment core site makes it possible to interpret terrigenous depositional signals from marine sediments. These signals include different continental weathering modes (i.e., physical vs. chemical) and spatiotemporal changes in rainfall patterns. However, local erosional products can be mixed with more distal ones transported by wind and/or oceanic currents, complicating the depositional signal at a site (e.g., Blanchet et al., 2021; Dinis et al., 2020; Garzanti et al., 2014; Hahn et al., 2018; He et al., 2020; Maccali et al., 2018; Meyer et al., 2011). Therefore, to reconstruct terrestrial climate variability from marine sediments near continental margins, it is essential to accurately fingerprint the provenance of these terrigenous materials, that is, which catchment area they integrate and their respective transport routes.

Various proxies have been used to decipher terrigenous sediment input to the marine realm, with sediment geochemistry and clay mineralogy proving to be the most effective (Beny et al., 2020; Chen et al., 2020; Dinis et al., 2020; Garzanti et al., 2014; Goldstein et al., 1984; Grousset et al., 1988, 1998; Hahn et al., 2018; He et al., 2020; van der Lubbe et al., 2014, 2016). The  $^{87}\text{Sr}/^{86}\text{Sr}$  and  $^{143}\text{Nd}/^{144}\text{Nd}$  values of weathering products, which display variations due to the radioactive decay of long half-life isotopes of  $^{87}\text{Rb}$  and  $^{147}\text{Sm}$ , are widely recognized and effective tools for determining the sources of lithogenic fractions in terrigenous detrital sediment found in marine deposits (Goldstein et al., 1984; Grousset & Biscaye, 2005; Hu et al., 2012). The  $^{143}\text{Nd}/^{144}\text{Nd}$  isotopic signature, expressed as  $\epsilon\text{Nd}$  [ $^{143}\text{Nd}/^{144}\text{Nd}$  normalized to the Chondritic Uniform Reservoir (CHUR) in parts per 10,000] (Jacobsen & Wasserburg, 1980), is commonly considered the most reliable provenance tracer as its values are not readily altered during processes such as sediment transport and chemical weathering (Blum & Erel, 2003; Fagel et al., 2004; Fagel, 2007; Garzanti et al., 2014; Goldstein et al., 1984; Grousset et al., 1988, 1998; Hahn et al., 2016, 2018; van der Lubbe et al., 2016; Meyer et al., 2011). In contrast, numerous studies have shown that  $^{87}\text{Sr}/^{86}\text{Sr}$  values can reflect various grain-size and weathering effects in addition to tracing sediment provenance (e.g., Blum & Erel, 2003; Dasch, 1969; Feng et al., 2009; Grousset et al., 1992; Meyer et al., 2011). This occurs because strontium (Sr) becomes more mobile during chemical weathering and is consequently removed from the source material. This increases the Rb/Sr ratio and consequently,  $^{87}\text{Sr}/^{86}\text{Sr}$  increases in the weathered rock (Blum & Erel, 2003; Jung et al., 2004; Meyer et al., 2011).

Geochemical and isotopic analysis of river sediments have been conducted for numerous localities across southern Africa (e.g., Dinis et al., 2020; Garzanti et al., 2014; Hahn et al., 2016, 2018; Herbert, 2009; Weldeab et al., 2013). However, their spatial coverage remains sparse and is often focussed on coarse-grained sediment fractions that are less likely to be transported to deep marine basins. Along the southeast African coastline, provenance studies are limited to within and offshore of the Limpopo River catchment (e.g., Garzanti et al., 2014; Simon et al., 2020a) and to the north offshore of the Zambezi catchment (van der Lubbe et al., 2016). Specifically within South Africa, several studies have identified the terrestrial geochemical signals in the marine environment by linking terrigenous sediment samples and marine core sites (e.g., Hahn et al., 2016, 2018) and offshore southwestern rivers such as the Orange River (Compton & Maake, 2007; Weldeab et al., 2013). These studies have successfully coupled marine lithogenic sediments with generalized drainage basins rather than individual source lithologies. In southern-eastern Africa, most of the geochemical and isotopic studies which have been carried out so far on riverine sediments are from the coarse-grained fraction sands ( $>63\ \mu\text{m}$ ) and gravels ( $>2\ \text{mm}$ ), which are not directly comparable to the fine-grained ( $<63\ \mu\text{m}$ ) deep marine sediment (Hjulström, 1955). The lithogenic clay fraction ( $<2\ \mu\text{m}$ ) is used as it has been previously recognized to be a faithful indicator of transport processes of suspended sediments (Bayon et al., 2015; Chamley, 1989; Walter et al., 2000), and therefore its ability to be transported over large distances and to integrate substantial source areas. Additionally, the  $2\text{--}32\ \mu\text{m}$  fraction is used to provide consistency with previous studies that analyzed the  $<32\ \mu\text{m}$  fraction (Garzanti et al., 2014). Here, for the first time, a consistent and systematically sampled transect from northeast South Africa (Durban) to southwest (Cape Town) is presented. This allows for establishing accurate land-sea linkages and deciphering terrigenous input to the marine realm.

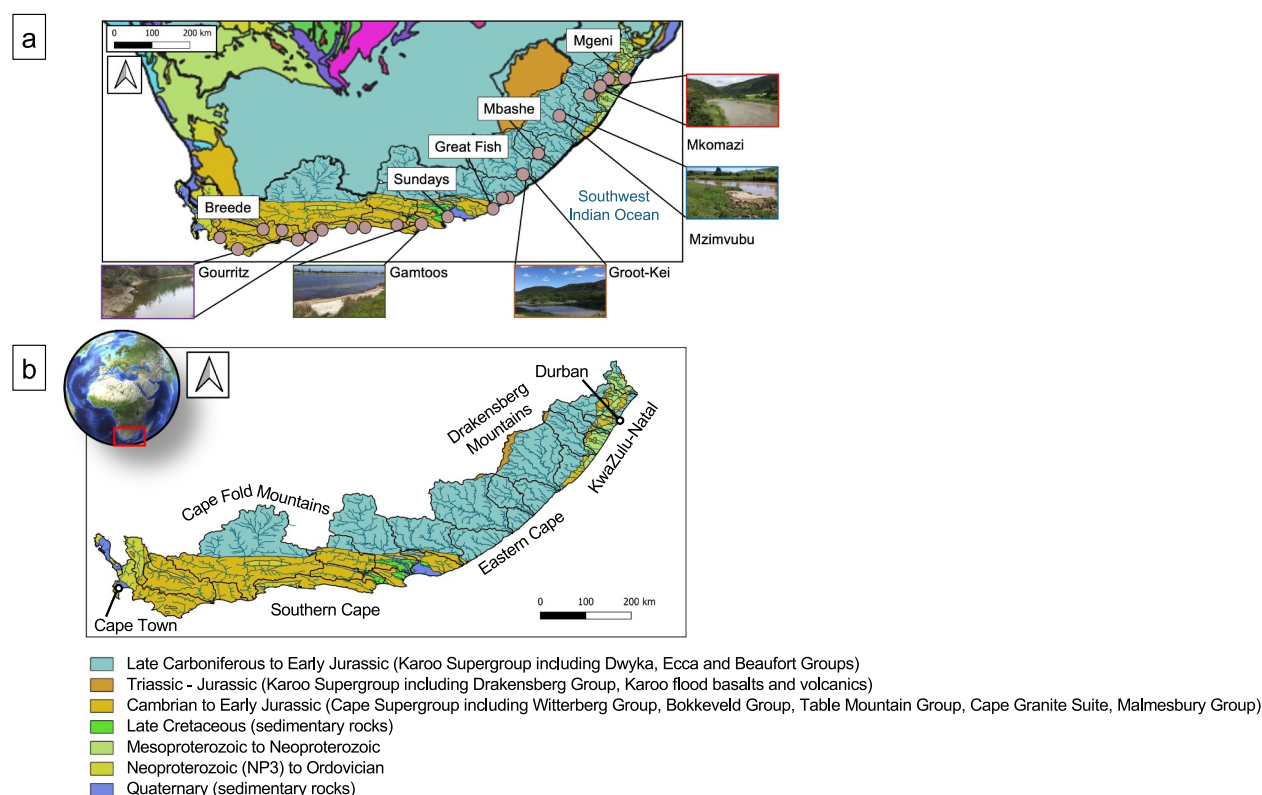


**Figure 1.** (a) Geology map of Southern Africa with major river drainage areas and sample locations (beige circles). Rivers photographed (red, Mkomazi; blue, Mzimvubu; orange, Groot-Kei; green, Gamtoos; purple, Gourits). Other major rivers labeled are Mgeni, Mbashe, Great Fish, Sundays and Breede. (b) South African bedrock geology within each drainage basin, with legends indicating the ages of bedrock types. Key locations and provinces are discussed in the text. Geology base map from Thieblemont (2017). River drainage networks from the Global Runoff Data Centre (GRDC) HydroRIVERS data set and the drainage basin extent from the Hydro1K data set were applied to obtain the drainage basins from the GRDC Major River Basins (MRB) of the World, incorporating data sets from the HydroSHEDS database.

### 1.1. Regional Geology and Fluvial Systems

The regional geology surrounding Durban (in the KwaZulu-Natal) and the Eastern Cape differs considerably from the Southern Cape (Figure 1). The Karoo Supergroup is the prominent bedrock type in the Eastern Cape. It overlies the older Cape Supergroup, which forms southern Africa's most extensive geological series. It is central to the Drakensberg Mountain system (Stewart et al., 2020) and extends East-West across central South Africa (Figure 1). The topographic lower parts of the Karoo Supergroup are composed of the Dwyka, Ecca and Beaufort Groups from the lower Carboniferous to Early Jurassic (Catuneanu et al., 2005; Moore et al., 2009; Neumann et al., 2011; Riley et al., 2005), which consist mainly of mud- and silt stones. These sedimentary rocks are capped by the Drakensberg Group, a succession of basalts such as the Karoo basalts (Compton, 2004). The KwaZulu-Natal region is additionally cut by numerous dolerite dykes and sills (Riley et al., 2005).

The Cape Supergroup is an Early Paleozoic unit (Cambrian-Ordovician) and extends ~1,000 km across the Southern and Western Cape of South Africa. It is subdivided into groups predominantly consisting of mudstone of the younger Witteberg and Bokkeveld Groups and sandstones and shales of the older Table Mountain Group (Compton, 2004). The oldest sequences are the Cape Granite Suite and Malmesbury Group, a metamorphosed shale. The Cape Granite Suite is stratigraphically below the Table Mountain Group (Harris et al., 1999). The latter rock units are part of the Cape Fold Belt Mountains, which traverse the Southern Cape from West to East. The Cape Supergroup mainly comprises micaceous rocks that weather to illite (Hahn et al., 2016). The weathering products of these distinct bedrock types are transported across the river catchment areas to be discharged and finally deposited into the ocean.

Between Durban and Cape Town, there are 10 significant major rivers draining into the Southwest Indian Ocean, which are Mgeni, Mkomazi, Mzimvubu, Mbashe, Groot-Kei, Great Fish, Sundays, Gamtoos, Gourits and Breede

(Figure 1). The eastern and southern coastline of South Africa comprises many smaller coastal river catchments with an average annual sediment yield of  $\sim 10 \times 10^6 \text{ m}^3/\text{year}$  supplied to the Southwest Indian Ocean (Flemming, 1981; Rooseboom et al., 1992).

The rivers along the Eastern Cape mainly drain the rocks of the Karoo Supergroup, although rivers located close to Durban drain rocks from the Dwyka, Eccca and Beaufort Groups capped by the Drakensberg Group (Figure 1). More recently, under anthropogenic climate change and land-use change, expansive gullies have been formed, which contribute to mass soil degradation and erosion (Birkett et al., 2016; Hoffman & Todd, 2000; Le Roux, 2007; Seutloali et al., 2016). The sediments within these eastern catchment areas are notably rich in iron (Fe) oxides. Previous studies (e.g., Simon et al., 2015; Ziegler et al., 2013) have shown the effect of on-land hydrological variability on sediment input to the marine realm, indicating terrigenous components supplied to the core site from regional river discharge. As such, these geochemical proxies can be used concertedly with this study to provide information on the sediment source supply to marine sediment cores.

Along the Southern Cape, the major rivers draining from the interior of South Africa and the Cape Fold Mountains are the Gamtoos, Gourits and Breede (Figure 1). Based on the catchment geology, these rivers primarily transport erosional products from the Cape Supergroup (Figure 1). Most of the river courses in the Southern Cape do not erode the Karoo Supergroup as the Cape Fold Mountain Belt acts as a geological barrier (Stewart et al., 2020). The Gourits River catchment has a significant runoff ( $488 \times 10^6 \text{ m}^3/\text{year}$ ; Maitre et al., 2009) with a catchment size of  $45,715 \text{ km}^2$ . This river catchment drains within the Klein Karoo vegetation region primarily composed of fynbos (Hahn et al., 2017), situated within the Swartberg Mountain Pass, which stands 2,000 m above sea level and is located within 100 km of the coast (Hahn et al., 2017). Another major river, the Breede River, has the fourth-largest annual runoff in South Africa (Taljaard, 2003). It flows 322 km southeast and discharges into the ocean near Cape Infanta on the south coast (Cawthra et al., 2020; Dupont et al., 2021). The transported sediments are partly sequestered in the delta plains and/or submarine delta fans, and the remaining sediment is transported to the adjacent upper continental slope from where it is further distributed downslope via submarine canyons and subsequently to the deep sea by ocean currents (Green, 2009; Hu et al., 2012).

## 1.2. Climate and Fluvial Systems in Southern Africa

### 1.2.1. Modern Climate of South Africa

A range of complex ocean-atmosphere interactions drives South Africa's hydroclimate. These include the influence of the South Atlantic high-pressure systems on the Benguela Upwelling and Southwest Africa climate and the easterly winds that carry warm, moist air from the Indian Ocean, affecting the Southeast Africa climate (Camberlin et al., 2001; Castañeda et al., 2016; Dupont et al., 2011; Goddard & Graham, 1999; Mason, 1995; Simon et al., 2015; Stager et al., 2011; Strobel et al., 2019; Tierney et al., 2013; Walker, 1990). This results in three seasonal rainfall zones—the summer (SRZ), winter (WRZ) and year-round (YRZ) rainfall zones (Chase & Meadows, 2007, Figure 2). The WRZ receives moisture from the latitudinal migration of the Southern Hemisphere westerlies. These westerlies are influenced by the Antarctic sea ice extent and South Atlantic Ocean sea surface temperatures (Compton, 2011; Dupont et al., 2021; Nash, 2017). Within the SRZ, precipitation occurs today mainly during the austral summer months (November to February) when the easterly trade winds transport tropical moist air from the Southwest Indian Ocean to southern Africa (Reason & Mulenga, 1999). Annual rainfall reaches up to 1,000 mm in the SRZ and ranges between 5 and 350 mm in the WRZ (Compton, 2011; Nash, 2017) (Figure 2). The YRZ (Figure 2) region between these zones receives rainfall in all seasons, influenced by the Southwest Indian and South Atlantic oceans. These changes in the mean rainfall and seasonality are expected to impact the provenance of riverine sediments discharged and ultimately deposited offshore southern Africa. Based on the amount and pattern of rainfall, it is likely that more continental weathering will likely occur in the SRZ than in the WRZ.

## 2. Sampling and Analytical Methods

### 2.1. Sample Selection

Modern river sediment samples ( $n = 22$ ) were collected from riverbanks of active and abandoned river channels covering each major South African river catchment between Durban and Cape Town (Figure 1). These rivers are generally short and have small catchment areas, averaging  $5,400 \text{ km}^2$ , and lack extensive tributary networks that



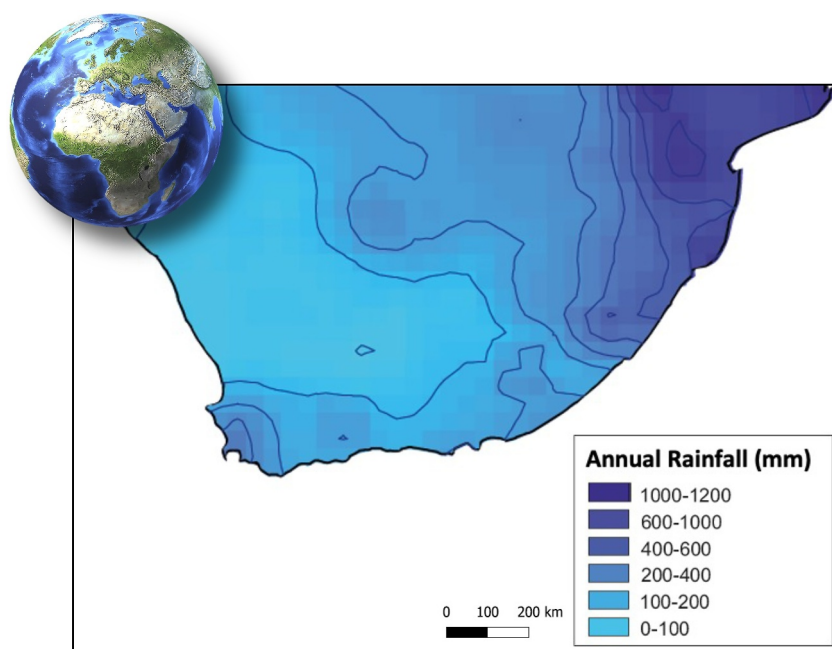


**Figure 2.** Annual mean rainfall map of South Africa, dotted lines display rainfall zones (labeled). WRZ corresponds to Winter Rainfall Zone, YRZ is Year-round Rainfall Zone, and SRZ is Summer Rainfall Zone. Data from Climate Research Unit (CRU), 50 km gridded resolution, smoothed to  $3 \times 3$  squares with contoured intervals.

transport sediment from more distant sources. This is in contrast to the large river basins to the north, including the Limpopo (408,000 km<sup>2</sup>) and Zambezi Rivers (1,390,000 km<sup>2</sup>) (Frenken et al., 1997). The rivers selected are complementary to the study of Hahn et al. (2017, 2018), which uses <63  $\mu$ m and <120  $\mu$ m size fractions on 10 rivers in South Africa. The overlap between the two studies applies to the Gourits River catchment, from which Hahn et al. (2017) analyzed eight samples in an upstream transect. However, their study did not include radiogenic isotopes from the Gourits River. Our study fills gaps in the existing data sets, cumulating into a complete data set from river samples on two specific grain size ranges from the Eastern and Southern Capes of South Africa, which are directly comparable to lithogenic sediment grain size fractions commonly found in deep-sea sediments.

Additionally, a potential issue with sampling southern African river catchments is that human activities, such as building dams that trap sediments upstream, increase surface erosion, and reduce river flow, can alter the natural radiogenic signature of sediments. Given the low relief of the downstream areas sampled, the river bank deposits collected downstream of the dam would still be representative of the upstream signal integrated prior to the dam being built when sediment transport was still active. However, this needs to be considered when analyzing riverine sediments to understand their origin and incorporation into the marine environment during the past.

The 22 sampled river catchments (Figure 1) have two main bedrock types: the Karoo and Cape Supergroups. To estimate the percentage bedrock type in each river catchment, the sampled rivers' drainage networks were defined using the Global Runoff Data Centre (GRDC) HydroRIVERS data set (Lehner & Grill, 2013). The Global 30 Arc-Second Elevation data set (GTOPO30) and Hydro1K data set were applied to obtain the drainage basins from the GRDC Major River Basins (MRB) of the World, incorporating data sets from the HydroSHEDS database. A geological map was obtained from the French Bureau de Recherches Géologiques et Minières (BRGM) geological survey (Thieblemont, 2017) and was overlaid by the catchment boundaries using the union tool in QGIS to quantify the central geological units within each drainage basin and the river catchment area was calculated based on the surface areas (Table S1 in Supporting Information S1).

## 2.2. Geochemistry—Pretreatment

In preparation for the radiogenic isotope (Sr and Nd) analysis, 20 g of each bulk riverine sediment sample ( $n = 22$ ) was washed and wet sieved at 63  $\mu$ m to separate the coarse (>63  $\mu$ m) and fine (<63  $\mu$ m) sediment fractions. The

samples were then sequentially leached and oxidized to remove organic carbon, carbonates, and Fe-Mn oxyhydroxides in order to isolate the detrital fraction (Bayon et al., 2002; Blaser et al., 2016; Gutjahr et al., 2007; Simon et al., 2020a, 2020b).

A total of 1 g of the <63  $\mu\text{m}$  dry fraction was placed in 40 mL of 2M acetic acid on a shaker table for >8 hr, allowing for direct comparison with the analyses of detrital sediments from marine sediment samples, which undergo decarbonization first to remove the marine carbonates. Hereafter, the samples were topped up with deionized (DI) water and left to settle overnight. The diluted acid was removed by siphon, and 20 mL of 6% hydrogen peroxide was added to the samples and placed on the shaker table for 6–8 hr. The samples were topped up with DI water and left to settle overnight. The supernatant was removed by siphoning, and samples were placed in 40 mL of buffered 1M acetic acid (pH  $\sim$  4) on a shaker table for >8 hr. The samples were topped up with DI water and left to settle overnight. The diluted acid was removed by siphoning, and the samples were transferred to 50 mL centrifuge tubes. Subsequently, 20 mL of 0.05 M hydroxylamine hydrochloride (HH) solution was added to the samples, and the samples were placed on the shaker table for at least 8 hr. The samples were centrifuged for 30 min (2,400 rotations per minute), and the clear HH solution was decanted. If the HH solution was colorless, only one leach was necessary. If the HH solution was (red/orange) tinted, the HH leaching was repeated until the supernatant appeared colorless. Samples were subsequently cleaned with DI water.

Following the sequential leaching, the samples were separated into two grain size fractions: <2  $\mu\text{m}$  and 2–32  $\mu\text{m}$ . The 2  $\mu\text{m}$  fraction was isolated using a centrifuge following Pryor et al. (2024). After analyzing the radiogenic isotopes in the <2  $\mu\text{m}$  fraction, an additional size separation was necessary for Sr isotopes to examine the grain size variations within separate size fractions. To separate the 2–32  $\mu\text{m}$  fraction, the residual sample material (>2  $\mu\text{m}$ ) was wet sieved using a <32  $\mu\text{m}$  sieve and dried at 40°C overnight. The <2  $\mu\text{m}$  fraction was selected for its capacity to represent the diverse bedrock found in the river catchment areas. Unlike coarser materials, its fine nature allows it to mix with and transport over long distances. The 2–32  $\mu\text{m}$  fraction was chosen to allow direct comparison with previous studies that analyzed the <32  $\mu\text{m}$  fraction (Garzanti et al., 2014).

### 2.3. Grain Size Analyses

Lithogenic grain size analyses were performed on the bulk sediment fraction at the Vrije Universiteit (VU) Amsterdam in the laboratory for sediment analyses using a Sympatec HELOS KR laser diffraction particle sizer, which allows grain size measurements in the range 0.12–2,000  $\mu\text{m}$  by 57 bins. To verify that all other components were removed successfully, microscope analyses were carried out on selected sediment samples before the grain-size analyses.

### 2.4. Radiogenic Sr and Nd Isotopic Analysis

Preparation and analysis of the radiogenic isotopes were performed at the School of Earth and Environmental Sciences, Cardiff University, in the Cardiff Environmental Laboratory for Trace Element and Isotope Chemistry (CELTIC). Approximately 20–50 mg of homogenized and powdered sample material from the two separate size fractions were completely dissolved in a mixture of concentrated HF-HNO<sub>3</sub> on a hotplate at 120°C for >24 hr; following evaporation to incipient dryness, the samples were taken up in 6M HCl and dried down. The samples were retaken up in 6M HCl and dried down before finally being dissolved in 8 M HNO<sub>3</sub>. The rock standard, JB2 Basalt (National Institute of Advanced Industrial Science and Technology) was processed alongside 22 samples and a procedural blank.

Strontium extraction from the sediment used Sr Spec resin, following a similar protocol to published methods (Charlier et al., 2006; Font et al., 2007; Scorrer et al., 2021). The <sup>87</sup>Sr/<sup>86</sup>Sr ratios were measured using a Nu Plasma II multi-collector inductively coupled plasma mass spectrometer (MC-ICP-MS) in CELTIC following methods in Scorrer et al. (2021). The total procedural blanks were typically less than 20 pg of Sr, a negligible result relative to the Sr in the samples (>20 ng). The repeated runs of the JB2 Basalt yielded a mean of  $0.70369 \pm 0.00010$  over two batches, compared to published JB2 values from the GeoREM database with a mean of 0.70368 ( $n = 32$ ). The Nd separation followed a 2-stage column separation using cation column exchange with AG-50W-X8 resin collecting the rare Earth elements and Nd separation via Ln-spec resin, using methods described in McCoy-west et al. (2017). The <sup>143</sup>Nd/<sup>144</sup>Nd ratio of the samples was measured on the Nu Plasma II MC-ICP-MS using the same methods as in Lambart et al. (2019). Typically, the procedural blanks were less than 100 pg of Nd, while the obtained  $\epsilon\text{Nd}$  values of  $+8.8 \pm 0.2$  for JB2 are consistent with literature data (Jochum

et al., 2005). Nd results are expressed as  $\epsilon\text{Nd}(0) = [((^{143}\text{Nd}/^{144}\text{Nd}_{\text{measured}})/0.512,638) - 1] \times 10,000$ , using the CHUR value given by Jacobsen and Wasserburg (1980).

## 2.5. X-Ray Diffraction (XRD)

Quantitative XRD measurements were completed on the clay fraction ( $<2\ \mu\text{m}$ ) samples using a Philips PW1710 Automated Powder Diffractometer at the Rock Preparation Facility, Cardiff University. Samples were prepared on glass slides (randomly orientated) and continuously scanned in  $2\theta$ - $\phi$  scanning mode from  $2$  to  $32^\circ\ 2\theta$  using the Philips PW1710 diffractometer with a CuK $\alpha$  radiation (35 kV voltage and 40 mA current). Quantitative mineral phase analysis was determined using the PW1877 APD version 3.6 software program via the graphical user interface PW1876 PC-Identify version 1.0b for identification. This is for the estimation of peak areas of the reflection for the main clay mineral groups of smectite (17 Å), illite (10 Å), and kaolinite/chlorite (7 Å). Relative clay mineral abundances are given in percentages. For consistency, all clay mineralogical data were identified based on the method of Biscaye (1965).

## 2.6. Endmember Modeling

### 2.6.1. Grain Size Endmember Generations

Weathering, transport, and deposition mechanisms favor specific characteristics such as grain size. Grain size endmember modeling is a metric for describing particle size distributions of possible sub-populations. Here, the grain size distributions of all samples were decomposed into discrete endmembers, allowing the significant terrigenous grain size components in the overall population to be identified, which are typically different transport processes and conditions. The resulting endmembers can be related to the grain-size distribution, potentially providing information on South African river systems' transport mechanisms and flow regimes. The grain size distributions of the total grain-size data set were decomposed into discrete endmembers using the Analyze package within MATLAB 2022b (Paterson & Heslop, 2015).

### 2.6.2. Sediment Source Endmember Mixing

The endmember mixing model used in this study requires two inputs: (a) the bedrock type in the studied river catchments and (b) the radiogenic isotope signatures from the corresponding river catchments. For the end-member generation for the  $<2\ \mu\text{m}$  fraction, the measured  $^{87}\text{Sr}/^{86}\text{Sr}$  and  $\epsilon\text{Nd}$  from that isolated size fraction were inputted, whereas for the  $2$ – $32\ \mu\text{m}$  endmembers, the  $^{87}\text{Sr}/^{86}\text{Sr}$  ratios measured from the  $2$ – $32\ \mu\text{m}$  fraction were used together with the  $\epsilon\text{Nd}$  from the  $<2\ \mu\text{m}$  fraction.

To determine the contribution of each bedrock lithology in each river catchment, the region was mapped using QGIS (Figure 1). The river catchment area was calculated based on the surface areas from the Hydro1K catchment data set. This allowed the spatial extent of each bedrock type within the catchment area to be calculated and the percentage bedrock of each river catchment to be determined. Based on this output, the bedrock age was calculated, which allowed the weighted average age of each catchment to be determined (Table S1 in Supporting Information S1). The percentages of the main geological units of South Africa in each river catchment (Table S1 in Supporting Information S1) were calculated from data outputted from QGIS and used in the mixing calculations, giving the proportion of the exposed area of the upstream lithology. The radiogenic Nd and Sr isotopic endmembers for the South African lithologies—Karoo and Cape Supergroup basement rocks were generated by inverting a simple mixing model to explain the isotopic composition of the river sediments. Each sample is assumed to be a mixture of only the Karoo Supergroup rocks and Cape Supergroup rocks.

For simplicity, the model assumes that the relative exposed areas of these lithologies within the upstream catchment correspond to the relative contribution to the mixing proportions that is, constant erosion rates across the basins. Furthermore, as there are no Nd and Sr concentration data from the river sediments available for this data set, the conservative assumption is made that the different endmembers possess the same Sr and/or Nd concentrations. Finally, the lithological supergroups are presumed to have the same composition across the studied region. Making these assumptions, the following expressions can be used for the isotopic composition of a sample  $i$ :

$$\epsilon\text{Nd}_i = A_{\text{karoo},i} \epsilon\text{Nd}_{\text{karoo}} + A_{\text{cape},i} \epsilon\text{Nd}_{\text{cape}}$$

$$Sr_i^{87} = A_{karoo,i} Sr_{karoo}^{87} + A_{cape,i} Sr_{cape}^{87}$$

where  $A$  is the exposed area of the given lithology upstream, and  $\epsilon Nd_{karoo}$ ,  $\epsilon Nd_{cape}$ ,  $Sr_{karoo}^{87}$  and  $Sr_{cape}^{87}$  are the endmember compositions. As there are multiple observations,  $n$ , it is possible to represent the resulting  $2n$  expressions in matrix form:

$$Ax = b$$

where  $A$  is a  $n \times 2$  matrix that gives the areas of each lithology,  $x$  is a  $2 \times 2$  matrix containing the endmember isotopic compositions of the two lithologies, and  $b$  is our  $n \times 2$  observations matrix of isotopic compositions. This equation can be inverted to find  $x$  given  $A$  and  $b$ .

To perform this inversion, a least-squares approach was applied to minimize the misfit between predictions and observations implemented using the NumPy Python package (Harris et al., 2020). Before solving the equation, the observations were normalized to vary between 0 and 1 to weight each isotope system equally. Therefore, the calculated endmembers are “consensus” endmembers that best fit all our observations downstream, given variable areal exposure upstream. Finally, the mixing trend was generated by fitting a two endmember mixing model to the sedimentary isotopic data using least squares. As the endmember concentrations of Sr and Nd are assumed to be equal, the mixing trend is linear in isotopic space (see Figure 6). Using existing Nd and Sr concentration data (Franzese et al., 2006), mixing lines were made to estimate the endmember concentration effect of Sr and Nd and weight the contribution of the endmembers.

### 3. Results

#### 3.1. Mineralogy and Geochemistry

To differentiate between the  $^{87}\text{Sr}/^{86}\text{Sr}$  ratios measured on clay fraction  $<2\ \mu\text{m}$  and the fine silt  $2\text{--}32\ \mu\text{m}$  fraction, the  $^{87}\text{Sr}/^{86}\text{Sr}$  signatures are hereafter referred to as  $^{87}\text{Sr}/^{86}\text{Sr}_{\text{clay}}$  and the  $^{87}\text{Sr}/^{86}\text{Sr}_{\text{finesilt}}$  ratios for  $<2\ \mu\text{m}$  and  $2\text{--}32\ \mu\text{m}$  fractions, respectively.

##### 3.1.1. $<2\ \mu\text{m}$ Fraction

Within the KwaZulu-Natal province,  $\epsilon Nd$  values are the most unradiogenic among the South African catchments, ranging between  $-12.50$  and  $-8.14$  ( $\pm 0.26$ , LPS03-06; Table 1). The  $^{87}\text{Sr}/^{86}\text{Sr}_{\text{clay}}$  ratios from the KwaZulu-Natal province vary from  $0.74151$  to  $0.74781$  ( $\pm 0.00001$ ).

In the rivers within the Eastern Cape (LPS11a—LPS24a; Table 1),  $\epsilon Nd$  ratios discriminate the younger Karoo sediments, with  $\epsilon Nd$  values  $> -8.90$  ( $\pm 0.18$ ) and  $^{87}\text{Sr}/^{86}\text{Sr}_{\text{clay}}$  ratios displaying values as low as  $0.72954$  ( $\pm 0.00001$ ). River sediment ratios within the Karoo Supergroup have a geologically younger  $^{87}\text{Sr}/^{86}\text{Sr}_{\text{clay}}$  fingerprint ( $0.72954\text{--}0.74717$  ( $\pm 0.00001$ )).

The Southern Cape rivers of the Cape Supergroup have a more extensive range of  $\epsilon Nd$  and  $^{87}\text{Sr}/^{86}\text{Sr}_{\text{clay}}$  ratios (LPS 28- LPS45; Table 1), with higher  $^{87}\text{Sr}/^{86}\text{Sr}_{\text{clay}}$  ratios ranging from  $0.73240$  to  $0.76615$  ( $\pm 0.00001$ ), compared to the rivers of the KwaZulu Natal and Eastern Cape. The  $\epsilon Nd$  values show a distinct difference between the drainage regions further south and those draining on the eastern coast. In the Southern Cape,  $\epsilon Nd$  values vary from  $-10.44$  to  $-8.94$  ( $\pm 0.24$ ) and are somewhat more unradiogenic than in the Eastern Cape ( $> -8.90$  ( $\pm 0.18$ )). These measured  $\epsilon Nd$  values from the Eastern Cape and Southern Cape are similar to the nearby  $\epsilon Nd$  endmember identified by Franzese et al. (2006) and other studies from South African rivers and offshore South Africa (e.g., Hahn et al., 2017; Herbert, 2009; Weldeab et al., 2013), which were all performed on various size fractions. However, the  $^{87}\text{Sr}/^{86}\text{Sr}_{\text{clay}}$  values vary significantly in these studies, which may be due to the differing size fractions. These results align with published literature that broadly suggests the  $\epsilon Nd$  isotope system is less sensitive to grain size and is a reliable provenance tracer (e.g., Blum & Erel, 2003; Fagel et al., 2004; Fagel, 2007; Garzanti et al., 2014; Goldstein et al., 1984; Grousset et al., 1988, 1998; Hahn et al., 2016, 2018; Meyer et al., 2011; van der Lubbe et al., 2016) and gave reason to measure Sr isotopes on a coarser grain size.



**Table 1**

*Results Table of Measured Radiogenic Isotope Data for Both the <2  $\mu\text{m}$  and 2–32  $\mu\text{m}$  Size Fractions (Sr Isotopes) and <2  $\mu\text{m}$  Fraction for  $\epsilon\text{Nd}$  From South African Rivers*

Sample	River	Latitude	Longitude	Location	$^{87}\text{Sr}/^{86}\text{Sr}_{\text{clay}}$	2se	$^{87}\text{Sr}/^{86}\text{Sr}_{\text{finesilt}}$	2se	$\epsilon\text{Nd}$	2se
LPS03	Mgeni	−29.798	30.959	KZN	0.74781	0.00001	0.73129	0.00002	−11.27	0.19
LPS04a	uMlazi	−29.810	30.500	KZN	0.74565	0.00001	0.74447	0.00001	−12.07	0.36
LPS05a	Mkomazi	−30.008	30.245	KZN	0.74151	0.00001	0.74840	0.00001	−8.14	0.20
LPS06	Mzimkulu	−30.258	29.944	KZN	0.74303	0.00001	0.72342	0.00001	−8.53	0.24
LPS11a	Mzimvubu	−30.850	29.070	E	0.73782	0.00001	0.71735	0.00002	−7.83	0.26
LPS14	Mbashe	−31.920	28.448	E	0.72954	0.00001	0.72018	0.00001	−8.40	0.21
LPS15	Groot-Kei	−32.508	27.987	E	0.73771	0.00001	0.71642	0.00001	−8.61	0.22
LPS18	Tyolomnqua	−33.166	27.565	E	0.73163	0.00001	0.71379	0.00001	−7.84	0.22
LPS19	Keiskamma	−33.285	27.393	E	0.73461	0.00001	0.71140	0.00002	−7.61	0.19
LPS21	Groot-vis	−33.489	27.124	E	0.74223	0.00001	0.71225	0.00002	−8.24	0.22
LPS24a	Sundays	−33.711	25.798	E	0.74717	0.00001	0.71270	0.00001	−8.90	0.18
LPS28	Gamtoos	−33.922	25.027	S	0.74347	0.00001	0.72677	0.00001	−10.15	0.25
LPS29	Krom	−33.945	24.318	S	0.73581	0.00002	0.73314	0.00001	−10.44	0.22
LPS32	Keurbooms	−34.012	23.391	S	0.74476	0.00002	0.72609	0.00001	−9.68	0.22
LPS33	Kynsa	−34.020	22.996	S	0.73240	0.00002	0.72287	0.00001	−9.96	0.19
LPS37b	Kleinbrak	−34.087	22.134	S	0.74092	0.00002	0.73246	0.00001	−9.89	0.22
LPS38a	Gourits	−34.283	21.827	S	0.75613	0.00001	0.73193	0.00001	−9.36	0.19
LPS38b	Gourits	−34.283	21.827	S	0.75982	0.00001	0.72780	0.00001	−8.94	0.24
LPS39	Goukou	−34.364	21.416	S	0.76615	0.00001	0.75146	0.00002	−9.97	0.31
LPS41	Duisenhoks	−34.096	20.966	S	0.74636	0.00002	0.73011	0.00001	−9.45	0.30
LPS42	Bree	−34.067	20.414	S	0.74852	0.00001	0.73795	0.00001	−10.17	0.24
LPS45	Bot	−34.300	19.158	S	0.73788	0.00002	0.73070	0.00001	−9.34	0.25

*Note.* Note for Location, KZN, KwaZulu-Natal; E, Eastern Cape and S, Southern Cape.

### 3.1.2. 2–32 $\mu\text{m}$ (Fine Silt) Fraction

Sr isotope measurements were also conducted on the 2–32  $\mu\text{m}$  fraction as the grain size effect is more significant in  $^{87}\text{Sr}/^{86}\text{Sr}$  compared to that of  $\epsilon\text{Nd}$  (e.g., Bayon et al., 2009; Feng et al., 2009; Meyer et al., 2011). The  $^{87}\text{Sr}/^{86}\text{Sr}_{\text{finesilt}}$  ratios from the KwaZulu-Natal are predominantly lower than the  $^{87}\text{Sr}/^{86}\text{Sr}_{\text{clay}}$  values. The  $^{87}\text{Sr}/^{86}\text{Sr}_{\text{finesilt}}$  ratios have a more extensive range from 0.72342 to 0.74840 ( $\pm 0.00001$ ) in the KwaZulu-Natal region than the  $^{87}\text{Sr}/^{86}\text{Sr}_{\text{clay}}$  from the co-registered sample (Figure 3). One exceptional value is identified from the Mkomazi River (LPS05a) as the  $^{87}\text{Sr}/^{86}\text{Sr}_{\text{finesilt}}$  value is more radiogenic than the clay fraction (Figure 3). Sediments from the Eastern Cape (e.g., Mzimvubu, Mbashe, Groot-Kei, Tyolomnqua, Keiskamma, Groot-vis and Sundays) carry a lower  $^{87}\text{Sr}/^{86}\text{Sr}_{\text{finesilt}}$  values by 0.02237 than the corresponding  $^{87}\text{Sr}/^{86}\text{Sr}_{\text{clay}}$  values. The  $^{87}\text{Sr}/^{86}\text{Sr}_{\text{finesilt}}$  versus  $^{87}\text{Sr}/^{86}\text{Sr}_{\text{clay}}$  values within the Southern Cape are 0.01463 lower. Overall, for all samples measured, the average offset between the  $^{87}\text{Sr}/^{86}\text{Sr}_{\text{clay}}$  values and the  $^{87}\text{Sr}/^{86}\text{Sr}_{\text{finesilt}}$  values is +0.01582, but differences range between 0.03447 and 0.00117 (Figure 3).

### 3.2. Grain Size

The riverine sediments exhibit unimodal or polymodal grain size distributions reflecting varying energies and bedload fractions, with a mean grain size of 160  $\mu\text{m}$ . Generally, sediments originating from the Karoo Supergroup are finer-grained than those from the Cape Supergroup. Karoo sediments have an average grain size of 88  $\mu\text{m}$ , compared to the Cape Supergroup, which has a mean grain size of 238  $\mu\text{m}$  (Figure S1a in Supporting Information S1).

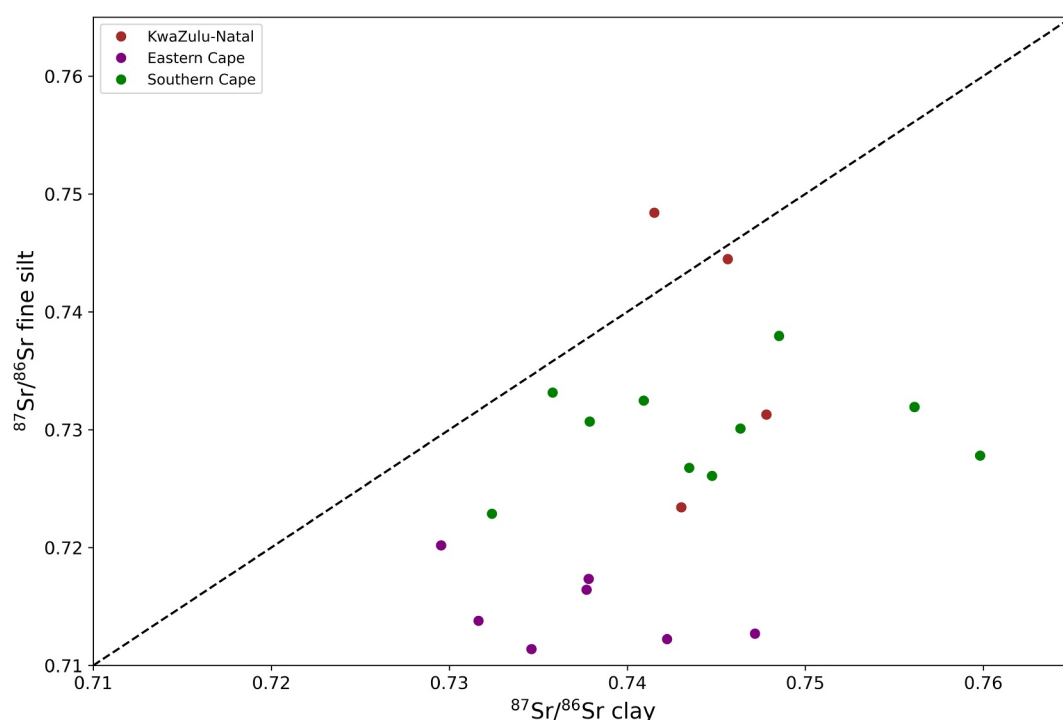


**Figure 3.** Comparison of  $^{87}\text{Sr}/^{86}\text{Sr}$  isotope ratios from the  $<2\ \mu\text{m}$  (clay) and  $2\text{--}32\ \mu\text{m}$  (fine silt) size fractions. KwaZulu-Natal (brown), Eastern Cape (purple) and Southern Cape (green). Black dashed line is a 1:1 ratio.

The grain size of all riverine sediment samples can be unmixed (decomposed) into three endmembers, showing a strong fit with an  $r^2$  value of 0.89 between the measured and modeled grain-size distributions. The finest grain-sized endmember has a distribution centered around  $44\ \mu\text{m}$  (Figure S1b in Supporting Information S1) and is likely to be the suspension mode of these dominantly seasonal rivers. The mode of the coarsest-grained endmember is centered around  $350\ \mu\text{m}$  and, therefore, represents riverine bedload transport (Figure S1b in Supporting Information S1).

### 3.3. Clay Mineralogy

River sediments from the KwaZulu-Natal (LPS03–LPS06; Table 2) have high kaolinite abundances (between 44% and 57%). Within the Eastern Cape (LPS11a–LPS24a; Table 2), sediments have lower kaolinite ( $<26\%$ ) and more illite compositions than the KwaZulu-Natal. Clay assemblages from the Southern Cape (LPS28–45) feature high abundances of illite. However, sample LPS 45 (Bot River) has a higher kaolinite composition (60.1%), making it more closely aligned with the KwaZulu-Natal region.

### 3.4. Sediment Source Endmember Mixing

The  $^{87}\text{Sr}/^{86}\text{Sr}$  and  $\epsilon\text{Nd}$  values of each river sample along with the respective bedrock type in each corresponding river catchment area were employed to identify potential endmembers for  $^{87}\text{Sr}/^{86}\text{Sr}$  and  $\epsilon\text{Nd}$  from the  $<2\ \mu\text{m}$  fraction according to the mixing model detailed above (Section 2.6.2; Figure 4). This model identified two  $<2\ \mu\text{m}$   $^{87}\text{Sr}/^{86}\text{Sr}$  and two  $\epsilon\text{Nd}$  endmembers for the Karoo and Cape Supergroups.

The  $\epsilon\text{Nd}$  data demonstrate a clear mixing signal between the two identified endmembers (Figure 4b) with most data situated close to the modeled mixing line. However, there are two localities from the KwaZulu-Natal where the  $\epsilon\text{Nd}$  predictions deviate from the measured data, which may indicate the presence of an additional endmember. Overall, the  $\epsilon\text{Nd}$  mixing supports previous studies regarding the reliability of  $\epsilon\text{Nd}$  as a provenance tracer (Blum & Erel, 2003; Fagel, 2007; Fagel et al., 2004; Garzanti et al., 2014; Goldstein et al., 1984; Hahn et al., 2016, 2018; He et al., 2020; Meyer et al., 2011; van der Lubbe et al., 2016). In contrast, the  $^{87}\text{Sr}/^{86}\text{Sr}_{\text{clay}}$  (Figure 4b) values deviate more significantly from the assumed mixing line, suggesting other processes are influencing the Sr signal in addition to source inputs from the Karoo and Cape Supergroups. To better constrain the Sr isotopes

**Table 2**

*Clay Mineral Abundances for River Sediment Samples (LPS03-LPS06 From KwaZulu-Natal, LPS11a to LPS24a From Eastern Cape and LPS28 to LPS45 Are From Southern Cape)*

Sample	River	Latitude	Longitude	Kaolinite (%)	Illite (%)	Montmorillonite (%)
LPS03	Mgeni	−29.798	30.959	44.5	53.0	2.5
LPS04a	uMlazi	−29.810	30.500	51.3	47.1	1.6
LPS05a	Mkomazi	−30.008	30.245	45.5	52.8	1.7
LPS06	Mzimkulu	−30.258	29.944	57.3	37.1	5.6
LPS11a	Mzimvubu	−30.850	29.070	18.8	81.1	0.1
LPS14	Mbashe	−31.920	28.448	9.9	87.2	2.9
LPS15	Groot-Kei	−32.508	27.987	26.8	70.3	2.9
LPS18	Tyolomnqua	−33.166	27.565	20.3	78.9	0.8
LPS19	Keiskamma	−33.285	27.393	8.2	90.7	1.1
LPS21	Groot-vis	−33.489	27.124	17.5	81.3	1.2
LPS24a	Sundays	−33.711	25.798	9.9	88.7	1.4
LPS28	Gamtoos	−33.922	25.027	13.0	85.1	1.9
LPS29	Krom	−33.945	24.318	58.8	34.8	6.4
LPS32	Keurbooms	−34.012	23.391	35.9	61.3	2.8
LPS33	Kynsa	−34.020	22.996	42.4	55.0	2.6
LPS37b	Kleinbrak	−34.087	22.134	29.9	65.9	4.1
LPS38a	Gourits	−34.283	21.827	16.4	83.0	0.6
LPS38b	Gourits	−34.283	21.827	19.0	80.2	0.8
LPS39	Goukou	−34.364	21.416	20.7	74.9	4.4
LPS41	Duisenhoks	−34.096	20.966	25.2	69.4	5.4
LPS42	Bree	−34.067	20.414	27.9	68.6	3.4
LPS45	Bot	−34.300	19.158	60.1	38.5	1.4

systematics, the 2–32  $\mu\text{m}$  fraction was also measured for Sr isotopes to understand the Sr isotopes systematics. The model defines two  $^{87}\text{Sr}/^{86}\text{Sr}$  endmembers from the 2–32  $\mu\text{m}$  group for the Karoo and Cape Supergroup lithologies.

## 4. Discussion: Geochemical Fingerprints

### 4.1. Signals From the Radiogenic Isotopes

The  $\epsilon\text{Nd}$  endmember data show a significant difference between the Karoo Supergroup ( $-8.53 \pm 0.22$ ) and Cape Supergroup ( $-10.09 \pm 0.24$ ; Table 3). This observed difference in all  $\epsilon\text{Nd}$  values can be explained by the distinct geology in the region, with older bedrock correlating with more unradiogenic  $\epsilon\text{Nd}$  ( $r^2 = -0.82$ ) (Figure S2; Table S1 in Supporting Information S1, Pryor et al., 2024). Samples from the KwaZulu-Natal have an older  $\epsilon\text{Nd}$  signature (more unradiogenic), whereas most of the Eastern Cape is composed of the younger Karoo Supergroup extending along the eastern coastline of South Africa, with the river catchments cut off at the interior by the Drakensberg Mountains. Along the Southern Cape, the more unradiogenic  $\epsilon\text{Nd}$  values that we obtained reflect the older Cambrian-Ordovician basement rocks of the Cape Supergroup, which extends east-west across the Southern Cape region (Figure 5). This confirms that the  $\epsilon\text{Nd}$  primarily reflects the bedrock geology and is therefore a reliable provenance indicator, as widely suggested by previous studies (Blum & Erel, 2003; Fagel, 2007; Fagel et al., 2004; Garzanti et al., 2014; Goldstein et al., 1984; Hahn et al., 2016, 2018; He et al., 2020; Meyer et al., 2011; van der Lubbe et al., 2016). The two  $\epsilon\text{Nd}$  predictions that deviate from the observed data come from the KwaZulu-Natal region and may be explained by an additional endmember such as the Drakensberg Group, which we have not accounted for in the simple mixing model. Direct Sr and Nd isotope analyses of the Karoo Supergroup dolerites have been conducted (e.g., Neumann et al., 2011; Riley et al., 2005), with the Underberg Dykes, which are part of the Drakensberg Group range, exhibiting  $\epsilon\text{Nd}$  values between  $-14.50$  and  $1.10$  (Riley

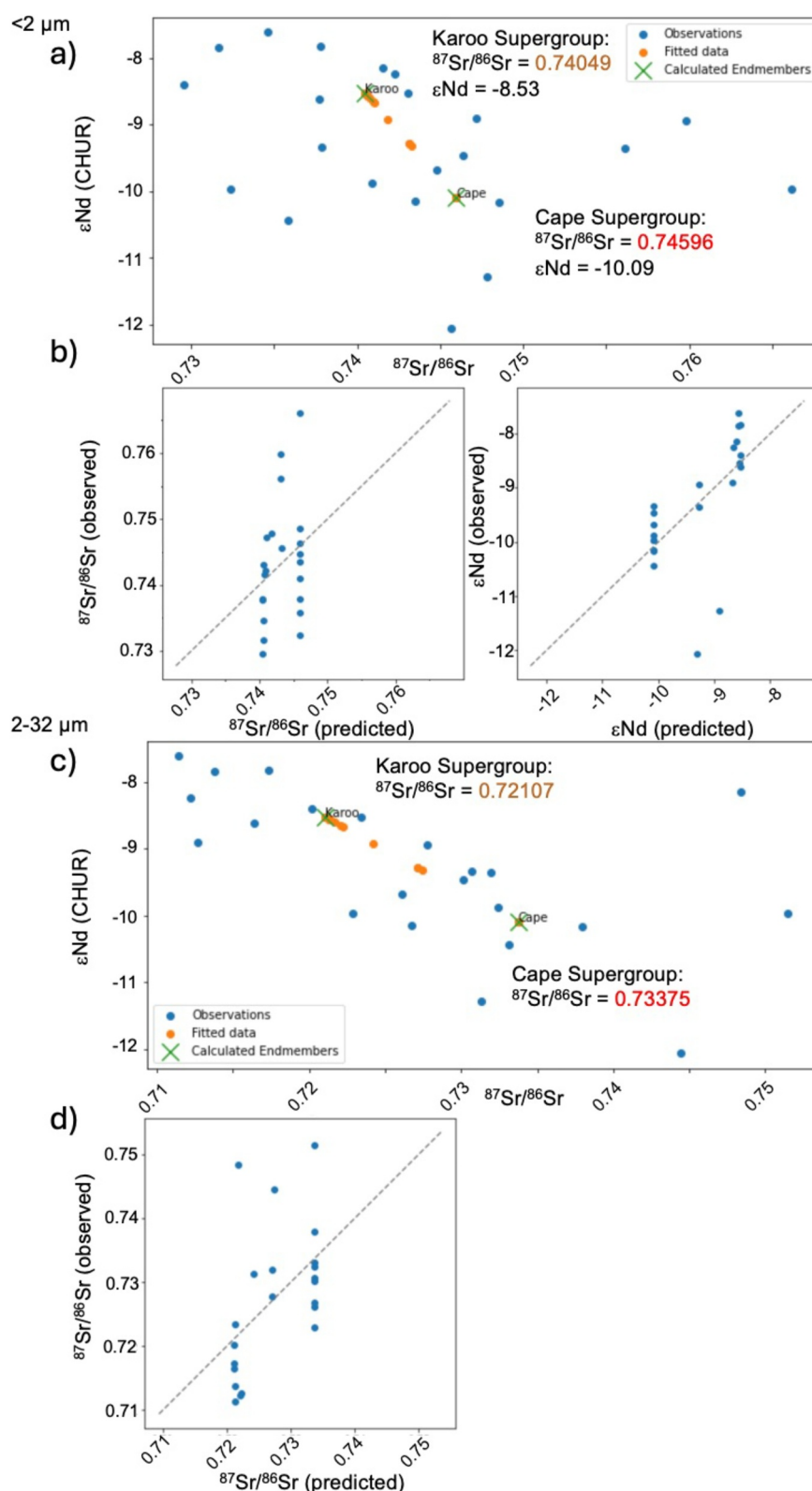


**Figure 4.** Radiogenic isotope endmember mixing calculation results for size fractions <2 μm (a, b) and 2–32 μm (c, d). The calculated endmembers for the Karoo and Cape are plotted as green crosses in (a, c) panels. Panels (b, d) present the data fit (blue filled circles) with the model prediction (straight dotted mixing line). Note the  $\epsilon_{\text{Nd}}$  endmember in (c) is generated using <2 μm data and  $\epsilon_{\text{Nd}}$  model fit is missing in panel (d) because there is no  $\epsilon_{\text{Nd}}$  available for 2–32 μm.

**Table 3**

Calculated Endmember Values for South African River Mud From Two Regions (Karoo Is Eastern Cape and Cape Is Southern Cape) Using the Radiogenic Isotope Mixing Model (Section 3.4)

Location	$^{87}\text{Sr}/^{86}\text{Sr}$ value	$\epsilon\text{Nd}$ value
Karoo	0.74049	−8.53
Cape	0.74596	−10.09

clear mixing signal (Figure 3) as the predicted signals deviate from the measured values based on catchment geology (Figure 4). This indicates that other factors are likely influencing the Sr isotope values.

## 4.2. Influences on the $^{87}\text{Sr}/^{86}\text{Sr}$ Ratios

### 4.2.1. Grain Size Effect on $^{87}\text{Sr}/^{86}\text{Sr}$ Ratios

All clay samples display a more radiogenic (higher)  $^{87}\text{Sr}/^{86}\text{Sr}_{\text{clay}}$  value than the  $^{87}\text{Sr}/^{86}\text{Sr}_{\text{finesilt}}$  fraction (2–32  $\mu\text{m}$ ) on average by +0.01582 except from sample LPS05a from the Mkomazi River (Figure 3, Table 1). This difference is 0.00001 ( $e^{-5}$ ) orders of magnitude higher than the  $^{87}\text{Sr}/^{86}\text{Sr}$  measurement uncertainty usually considered significant (Biscaye & Dasch, 1971). This significant grain size-induced offset is supported by previous studies (Carter et al., 2020; Jonell et al., 2018; Meyer et al., 2011). One such study (Hahn et al., 2016) identified a +0.02—offset in  $^{87}\text{Sr}/^{86}\text{Sr}$  isotope data measured in the <2  $\mu\text{m}$  fraction compared to <120  $\mu\text{m}$  fraction. We obtained a smaller offset between <2  $\mu\text{m}$  and 2–32  $\mu\text{m}$ , compared to the offset from Hahn et al. (2016), which is in line with the smaller grain size range covered in this study. Therefore, it is necessary to isolate size fractions for independent studies, as bulk sediment samples would give a mixed signal of all size fractions.

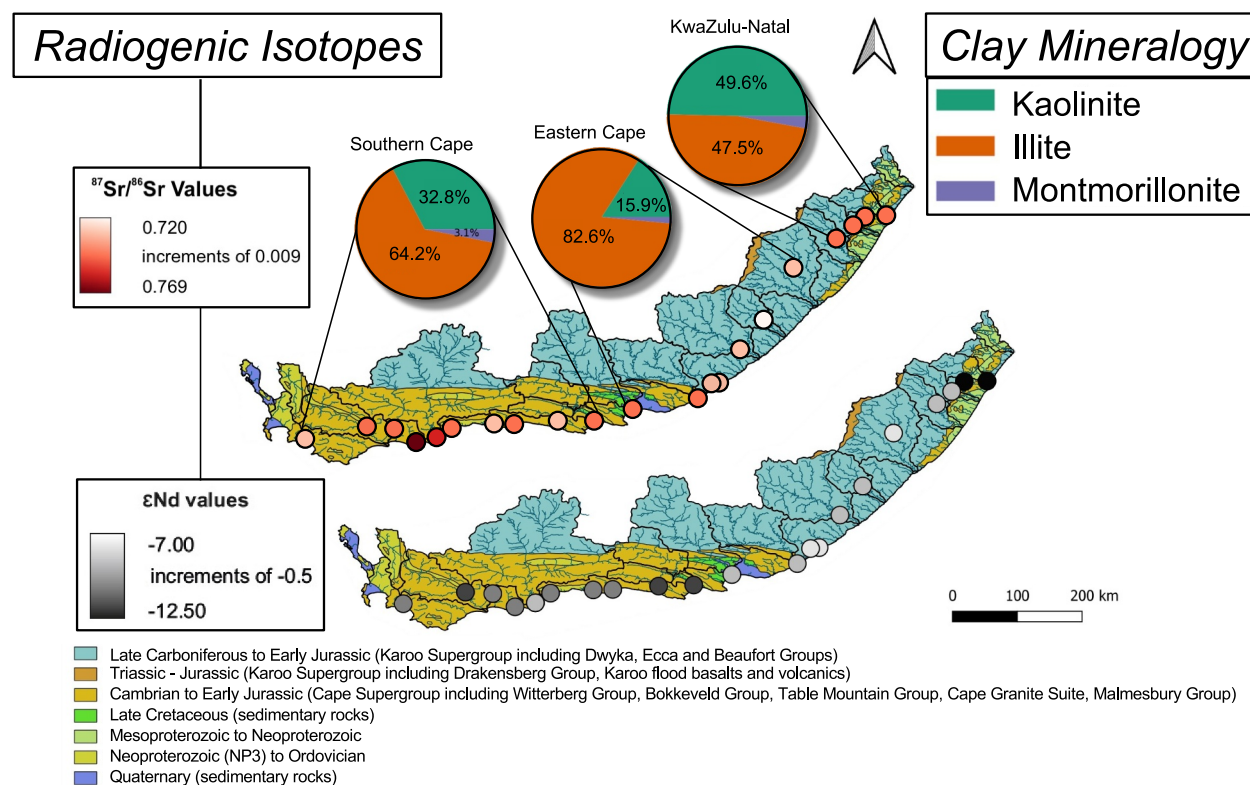


**Figure 5.** Radiogenic isotope compositions and clay mineralogies analyzed for sampled river catchments. The three pie charts represent the average clay mineral composition of three regions, KwaZulu-Natal ( $n = 4$ ), Eastern Cape ( $n = 7$ ) and Southern Cape ( $n = 11$ ) (top to bottom) (key on right). River catchment geology: circles indicate sample localities and circle color represents the radiogenic isotope values indicated by the keys (left).



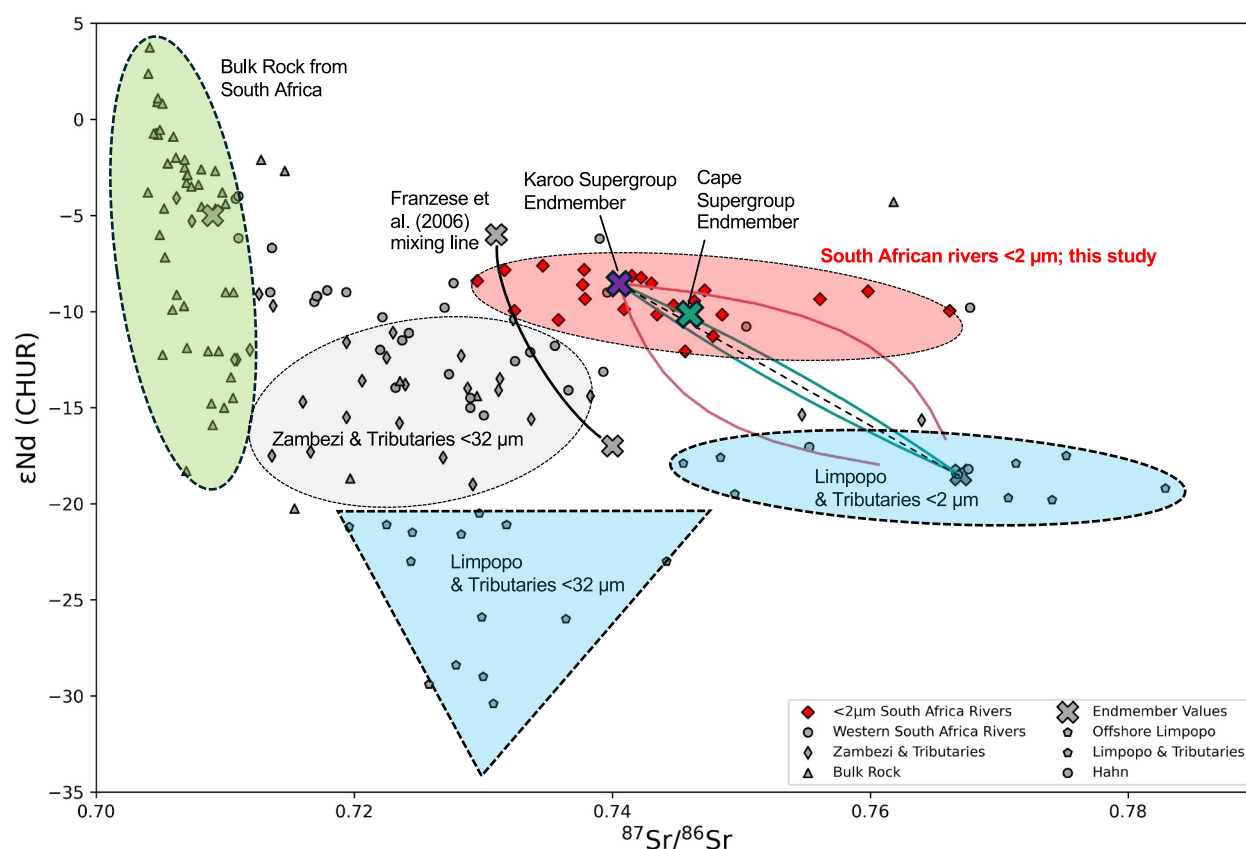


**Figure 6.** Sr-Nd isotope ratio mixing plot based on non-linear regression between South African river sediments (red) (Section 3.4) and published terrestrial and marine-derived samples from this region. Samples measured in this study are marked by red diamonds and discriminate from Limpopo and Zambezi sourced sediments. Generated Karoo Supergroup endmember, purple cross and Cape Supergroup endmember, green cross. Hypothesized mixing lines from samples of the same grain size (<2 μm) from South Africa (our study) and offshore Limpopo (Simon et al., 2020a) are also given assuming constant Sr and Nd concentrations (dashed black line). Sr-Nd concentrations from Franzese et al. (2006); mean ± standard deviation (green mixing line), extreme values (pink mixing line). A mixing line from Franzese et al. (2006) for local offshore South African and Agulhas endmembers is indicated. Data used for Limpopo and Tributaries <2 μm; Simon et al., 2020a, <32 μm Garzanti et al., 2014; Zambezi and Tributaries <32 μm Garzanti et al., 2014; Western South Africa Rivers (Hahn et al., 2017; Herbert, 2009; Weldeab et al., 2013); South Africa <120 μm (Hahn et al., 2017); whole rock and bulk samples from South Africa (Lutinen et al., 1998; Neumann et al., 2011; Riley et al., 2005).

#### 4.2.2. Changes in Chemical Weathering Regime

During chemical weathering, Sr is preferentially removed compared to Rb, with the source material retaining Rb-rich minerals (e.g., micas), increasing the Rb/Sr ratio and the  $^{87}\text{Sr}/^{86}\text{Sr}$  in the weathered rock over time (Blum & Erel, 2003; Jung et al., 2004; Meyer et al., 2011). Hence, the observed deviations in  $^{87}\text{Sr}/^{86}\text{Sr}_{\text{clay}}$  isotope values in the weathered material likely represent the degree of chemical weathering and heterogeneous distribution of formed Rb-rich minerals (Åberg et al., 1989; Blum & Erel, 1997, 2003; Blum et al., 1993; Capo et al., 1998; Dasch, 1969; Derry & France-Lanord, 1996; Jung et al., 2004). The endmember mixing model results (Figure 4) support this conclusion as the Sr isotopes are not only influenced by source rock provenance, unlike the Nd isotopes. Moreover, in the KwaZulu-Natal, the radiogenic  $^{87}\text{Sr}/^{86}\text{Sr}$  values of 0.74151–0.74781 ( $\pm 0.00001$ ) ( $n = 4$ ) suggest that the sediments from the KwaZulu-Natal are subjected to more intense chemical weathering than those further south, based on rainfall amounts within the SRZ (Figure 2). Evidence of high erosion rates in South Africa, particularly on the eastern Escarpment, ranges from 1.8 m/million years (Ma) to 24 m/Ma (Makhubela et al., 2021), indicating that erosion rates are linked to topography. This trend is also evident in the Drakensberg Mountains, where the higher (more radiogenic)  $^{87}\text{Sr}/^{86}\text{Sr}_{\text{clay}}$  ratio can be attributed to increased annual rainfall amounts (Åberg et al., 1989) (Figure 2) and subsequent intensity of chemical weathering in the Drakensberg Mountains and SRZ of South Africa. In the mixing model, erosion rates in the river basins are assumed to be constant and may explain the deviations in the predicted Sr values from the measured Sr data. The southeastern coastline of South Africa experiences more rainfall due to the elevated sea surface temperature (SST)

of the Southwest Indian Ocean, which advects warm moist air on land (Camberlin et al., 2001; Castañeda et al., 2016; Dupont et al., 2011; Goddard & Graham, 1999; Mason, 1995; Simon et al., 2015; Stager et al., 2011; Strobel et al., 2019; Tierney et al., 2013; Walker, 1990). Neoformed clays may also affect the Sr isotope composition (e.g., Dellinger et al., 2015), particularly in regions with higher chemical weathering, such as the SRZ where rainfall is greater (Compton, 2011; Nash, 2017). Increased rainfall enhances physical disaggregation and chemical weathering of sediments in this region, causing a higher  $^{87}\text{Sr}/^{86}\text{Sr}$  signal. The impact of chemical weathering is further explored through the interpretation of the river sediments' clay composition (Section 4.4).

### 4.3. Source Regions

Based on sediment source endmember mixing (Section 3.4), two new South African radiogenic Nd-Sr isotope endmembers have been identified, which are different from the northern Zambezi River and offshore of the Limpopo River (Figure 6). The endmember mixing model resulting from the Sr and Nd values of each river sample and the corresponding bedrock type agrees well with previous radiogenic isotope studies from the region (e.g., Herbert, 2009; Simon et al., 2020a; Weldeab et al., 2013). The non-linear mixing line fits between local South African rivers (this study) and offshore the Limpopo River (Simon et al., 2020a) (Figure 6). The mixing lines, based on Nd and Sr concentration data from Franzese et al. (2006), sit close to the linear mixing line, revealing that despite potential isotopic variability in bedrock, the linear mixing line generated explains the mixing between the Limpopo River and South African rivers. Both the Limpopo and Zambezi Rivers drain geologically older cratonic sediment (Eglington & Armstrong, 2004; Jelsma & Dirks, 2002), which explains the offset between the relatively unradiogenic Karoo sediments with lower radiogenic Sr isotope values and the radiogenic Sr isotope values from the offshore Limpopo sediments. The average isotopic composition of the tributaries of the Zambezi catchment (Garzanti et al., 2014; van der Lubbe et al., 2016) is less radiogenic than sediments offshore the Limpopo River ( $^{87}\text{Sr}/^{86}\text{Sr} = 0.72395 (\pm 0.00003)$  ( $n = 25$ ) and  $\epsilon\text{Nd} = -13.79 (\pm 0.20)$  ( $n = 40$ ). Nearshore the mouth of the Limpopo River, the  $^{87}\text{Sr}/^{86}\text{Sr}_{\text{clay}}$  yields average ( $n = 8$ ) values of 0.76684 ( $\pm 0.000012$ ) and  $\epsilon\text{Nd}$  values of  $-18.48 (\pm 0.07)$ , based on data from Simon et al. (2020a) and the radiogenic isotopes mixing calculations. A previous mixing line generated by Franzese et al. (2006) (Figure 6) (based on lithogenic sediment from marine sediments) also supports the values identified in our study. However, the local endmembers (identified as South African rivers) (Franzese et al., 2006) bear a somewhat more unradiogenic Sr isotope value than our newly defined endmembers (Table 3). This offset might be attributed to the grain size fractionation effect (Figure 6) as Franzese et al. (2006) analyzed the radiogenic isotopic compositions on the  $<63 \mu\text{m}$  lithogenic fraction in marine sediments. Additional factors which could explain the offset between the Franzese et al. (2006) marine-derived endmembers and this riverine study are the influence of marine strontium and authigenic clay formation resulting in a shift to lower  $^{87}\text{Sr}/^{86}\text{Sr}$  values in the  $<63 \mu\text{m}$  class or additionally because of marine barite affecting the  $^{87}\text{Sr}/^{86}\text{Sr}$  signal (Jewell et al., 2022). Using riverine sediments to generate radiogenic isotope endmembers reduces the effect of marine barite, whereas the marine-derived endmembers in Franzese et al. (2006) could be influenced by barite. In both studies, no barite removal was tested. Interestingly, the  $\epsilon\text{Nd}$  values from Karoo and Cape endmembers are not too different from the nearby marine endmember  $\epsilon\text{Nd}$  identified in Franzese et al. (2006) ( $\epsilon\text{Nd} = -6$ ), which gives further evidence that the  $\epsilon\text{Nd}$  isotope system is less sensitive to grain size and/or authigenic processes, as found in previous studies (e.g., Bayon et al., 2009; Meyer et al., 2011).

### 4.4. Clay Composition

Clay assemblages show a northeast-southwest trend in decreasing (or increasing) kaolinite (or illite) abundances (Figure 5). Karoo-sourced river sediment clays are dominated by felspar sourced weathering products (70%) (Compton & Maake, 2007). Our data show high kaolinite abundances in the riverine sediments from the KwaZulu-Natal (Table 2: LPS03 to 11a; Figure 5), which can be attributed to weathering of the feldspars within granites of the Karoo sediment. This is supported by previous work, which found granite weathers to form kaolinite in regions of rainfall rates averaging 800–900 mm per year (van der Merwe & Weber, 1963). A positive relationship has been previously reported between higher amounts of kaolinite and annual rainfall within a catchment in Southwest Africa (Dinis et al., 2020).

The KwaZulu-Natal region and the Drakensberg Mountains, situated within the SRZ, receive approximately 1,000 mm of rainfall annually, making it the highest in South Africa (Rooseboom & Annandale, 1981; Rooseboom et al., 1992) (Figure 2). The rivers from the KwaZulu-Natal have a high annual sediment yield (601–

1,000 tonnes/km<sup>2</sup>; Compton & Maake, 2007; Walling, 1984) compared to the lower yield from the Eastern Cape rivers. The high abundance of kaolinite in the KwaZulu-Natal Province can, therefore, be characteristic of the weathering of granites, coincident with higher <sup>87</sup>Sr/<sup>86</sup>Sr ratios and chemical weathering rates (Blum & Erel, 2003). High kaolinite abundances have been recorded on the eastern side of Maputo, Mozambique in sediments from Nelshoogte, suggesting sediments from this region and close to Lesotho are more kaolinite-rich (van der Merwe & Weber, 1963) than further south.

Considering a soil-type base map (Figure S3 in Supporting Information S1), more red-brown ferrallisol soils are identified in the KwaZulu-Natal region, aligning with more radiogenic <sup>87</sup>Sr/<sup>86</sup>Sr ratios (Figure S3 in Supporting Information S1) and higher kaolinite compositions in the KwaZulu-Natal region. This soil type indicates more chemical weathering in this area as opposed to the more fluvisols in the Southern Cape. The presence of weathering products in the soils infers high weathering rates (Garzanti et al., 2014; van der Merwe & Weber, 1963), which we couple with more kaolinite (inferred as a conversion of feldspars to kaolinite due to weathering) and more radiogenic <sup>87</sup>Sr/<sup>86</sup>Sr ratios in the KwaZulu-Natal region. Changes in land use and vegetation may also influence the weathering rates and soil composition, with more gullies observed in the KwaZulu-Natal region, suggesting enhanced erosion in this region. This would influence the Sr isotope ratios toward a more radiogenic signal, as the weathered rock contains increased Rb/Sr and <sup>87</sup>Sr/<sup>86</sup>Sr ratios (e.g., Blum & Erel, 2003; Jung et al., 2004; Meyer et al., 2011).

Some rivers in the Eastern Cape drain from the east flank of the Drakensberg (e.g., LPS 06 and 11a). These sediments have a different geochemical composition from those draining from the westerly flank of Drakensberg (Compton & Maake, 2007; Compton & Wiltshire, 2009). These westerly flank river sediments are dominated by volcanoclastic mud (Garzanti et al., 2013). The volcanoclastic mud would have a different radiogenic εNd isotopic signature from the Karoo sediments. Significant differences do not occur in radiogenic Sr and εNd isotope composition of rivers draining from the eastern flank of the Drakensberg Mountains (e.g., LPS 06 and 11a; Table 1) compared to those from the Eastern Cape, which do not have a Drakensberg sediment source (e.g., LPS 14 to 24a; Table 1). There are high smectite abundances in riverine mud derived from the weathering of the Karoo basalts from the westerly Drakensberg Mountains (Compton & Maake, 2007). These riverine muds are carried by the Orange River westward to the Southeast Atlantic. As our sediments contain small amounts of montmorillonite (<10%; Table 2), which is a specific mineral within the smectite group, this likely indicates that the rivers to the east of the Drakensberg Mountains do not share the same provenance as the Orange River and/or the volcanoclastic muds from the westerly flank.

Further south of Durban, Karoo sedimentary rock soils (Eastern Cape) are more commonly rich in illite (Compton & Maake, 2007). A regional difference in geology is expressed in the clay assemblages, with riverine sediments from the Eastern Cape containing more illite than further North. In general, the ratio between kaolinite and illite in the terrestrial sediments corroborates well with marine records from the region from previous studies (Kuhn & Diekmann, 2002; Petschick et al., 1996). Comparative studies show that offshore South Africa is within a high illite zone (Kuhn & Diekmann, 2002; Petschick et al., 1996), and marine sediment from the Cape Walvis Ridge offshore of South Africa also reveals high illite assemblages (Petschick et al., 1996). This is apparent in the Karoo and Cape Supergroup weathering products, which contain more illite.

The southern drainage basins mainly contain older rocks reflecting the Cape Supergroup. The Cape Supergroup primarily comprises micas, which weather to illite (Compton & Maake, 2007; Hahn et al., 2016). The Gourits and Goukou river drainage basins have the highest illite abundance (74.9%–83.0%) among all samples collected from the Southern Cape. The higher illite abundances are probably associated with a higher proportion of geologically old micas from basement rocks eroded along the course of these rivers and brought by tributaries (Hahn et al., 2016). Conversely, the river catchments closest to Cape Town have a clay assemblage analogous to the sediment from the KwaZulu-Natal Province, with high kaolinite and low illite abundances (e.g., van der Merwe & Weber, 1963). This is likely explained by the underlying bedrock in the Cape Town region and the geological contact between sandstones and Cape granite intrusion in the area, which has geochemically imprinted the river sediment (Harris et al., 1999).

This highlights the effectiveness of a multiproxy study utilizing Sr, Nd, and clay minerals, as radiogenic isotopes alone fail to capture the full picture of provenance. A straightforward endmember mixing model does not adequately elucidate the geological sources of river sediments, indicating that additional research is necessary to determine the extent of isotopic variability related to different geological sources and grain sizes. Nevertheless, Sr

isotopes hold significant potential as tracers for the provenance of past hydroclimate variability, provided they are analyzed consistently across a specific grain size fraction to ensure accuracy. When used alongside other isotopic systems within a multiproxy approach, Sr isotopes can enhance our understanding of sediment dynamics and historical climate patterns.

## 5. Implications for Palaeoclimate Reconstructions

Understanding the geochemistry of river sediment aids in reconstructing past environmental conditions and changes in the terrestrial landscape. These reconstructions are essential for interpreting marine sediment records, which preserve evidence of climatic and environmental shifts. Radiogenic isotope reconstructions can be related to past climate variability (e.g., Blanchet et al., 2021; Dinis et al., 2020; Garzanti et al., 2014; He et al., 2020; Maccali et al., 2018; Meyer et al., 2011) as more weathering suggests higher rainfall amounts (Åberg et al., 1989). Clay particles are mainly produced through geochemical processes, particularly weathering, and typically contain minerals such as kaolinite and illite. As the finest grain size fraction, clay particles are transported considerably longer distances and with a shorter transfer time than the coarse fraction transported with bedload (Carter et al., 2020; Granet et al., 2010). Studies have shown that the clay fraction better integrates the bedrock from the drainage area due to its extensive mixing over longer distances (Carter et al., 2020; Jonell et al., 2017). The radiogenic isotope data indicate that the  $^{87}\text{Sr}/^{86}\text{Sr}_{\text{clay}}$  instead reflects the degree of weathering, while the  $\epsilon\text{Nd}$  matches the composition of the parent source rock.

The obtained South African radiogenic Sr-Nd isotope endmembers presented here can support future studies on the provenance of riverine sediments in South Africa (Table 3 and Figure 6). These data suggest that the Karoo and Cape  $\epsilon\text{Nd}$  and  $^{87}\text{Sr}/^{86}\text{Sr}_{\text{clay}}$  endmembers are robust indicators of local South African provenance. They can therefore be used to provide an adequate understanding of fluvial discharge variability and source rock weathering from South Africa. As a result, the application of this study is relevant to paleoclimate studies based on marine sediment cores close to the continent as the geochemical compositions of the river sediments would document the rainfall patterns of South Africa. In addition, the  $^{87}\text{Sr}/^{86}\text{Sr}_{\text{clay}}$  ratios could indicate a more continental weathering in the SRZ than in the WRZ due to rainfall totals and seasonality. Rainfall seasonality thus affects the intensity of chemical weathering, combined with variations in river transport strength, influencing both the radiogenic isotope signal and the grain size. Finer grain sizes are observed in the rivers of the SRZ from the Karoo Supergroup compared to those from the Cape Supergroup, which may suggest prolonged weathering. This shows that the application of radiogenic isotopes demonstrates their utility in inferring hydroclimate variations and seasonal rainfall patterns. Finally, the South African radiogenic isotope endmembers could distinguish from the more radiogenic  $\epsilon\text{Nd}$  isotope values of two major northern rivers (Limpopo River and Zambezi River) upstream of the Agulhas current (Figure 6). Therefore, these radiogenic isotope endmembers can clarify upstream versus local sediment supply at more distal sediment core sites, which can help infer changes in rainfall, river discharge and/or sediment transport strength at a regional scale.

## 6. Conclusions

The provenance of river sediments along the coastal regions of South Africa has been determined through the application of bedrock geology unmixing techniques in conjunction with radiogenic isotope analyses. This has identified two principal endmembers characterized by  $\epsilon\text{Nd}$  and  $^{87}\text{Sr}/^{86}\text{Sr}$  ratios, providing insight into the dynamics of the regional river systems. Specifically, rivers in the Eastern Cape are influenced by bedrock derived from the Karoo Supergroup, exhibiting  $^{87}\text{Sr}/^{86}\text{Sr}$  ratios of 0.74049 and an  $\epsilon\text{Nd}$  value of  $-8.53 (\pm 0.22)$ . In contrast, rivers flowing through the Southern Cape drain landscapes are underpinned by the Cape Supergroup, which is associated with more radiogenic  $^{87}\text{Sr}/^{86}\text{Sr}$  isotopes of 0.74596 and unradiogenic  $\epsilon\text{Nd}$  values of  $-10.09 (\pm 0.24)$ .

The KwaZulu-Natal fluvial sediments display elevated radiogenic  $^{87}\text{Sr}/^{86}\text{Sr}_{\text{clay}}$  ratios and more unradiogenic  $\epsilon\text{Nd}$  signatures with a significant kaolinite component. The predominant soil type within these catchments is ferralsols, which indicate advanced chemical weathering processes. This region in the SRZ experiences substantial rainfall due to the high SSTs of the Indian Ocean, facilitating higher evaporation and moisture transport inland (Camberlin et al., 2001; Castañeda et al., 2016; Dupont et al., 2011; Goddard & Graham, 1999; Mason, 1995; Simon et al., 2015; Stager et al., 2011; Strobel et al., 2019; Tierney et al., 2013; Walker, 1990). Given this increased precipitation, a concomitant rise in chemical weathering intensity is anticipated, suggesting that  $^{87}\text{Sr}/^{86}\text{Sr}_{\text{clay}}$



ratios serve as effective recorders of regional hydrological processes. Along the eastern coastline, there is a notable decline in kaolinite abundance, while the composition of illite shows a corresponding increase toward the south. This transition aligns with lower  $^{87}\text{Sr}/^{86}\text{Sr}_{\text{clay}}$  ratios and higher  $\epsilon\text{Nd}$  values, reflecting the geological characteristics of the underlying bedrock in the catchment areas. The younger Karoo sediment predominates in the Eastern Cape, whereas the older Cape Supergroup in the Southern Cape is characterized by a more radiogenic  $^{87}\text{Sr}/^{86}\text{Sr}_{\text{clay}}$  isotope signature and an unradiogenic  $\epsilon\text{Nd}$  fingerprint.

Finally, the influence of different grain size fractions on provenance analyses needs to be carefully considered for palaeoclimate reconstructions, particularly when interpreting land-sea connections or comparing radiogenic isotope data sets (Meyer et al., 2011). Therefore, it is essential to accurately separate the grain size classes as a prerequisite for such studies (Pryor et al., 2024). The sensitivity of  $^{87}\text{Sr}/^{86}\text{Sr}$  compositions to grain size discrepancies has resulted in inconsistencies when comparing different core locations utilized for proxy-based provenance analyses. As such, limitations persist in the utility of Sr isotope data from the bulk sediment fraction or when comparing existing data from different grain size fractions (Hahn et al., 2016; Jewell et al., 2021; Kunkelova et al., 2022; Meyer et al., 2011; Simon et al., 2020a).

## Data Availability Statement

See Pryor (2024) for data from Table S1 in Supporting Information S1 and grain size data measured on a Sympatec HELOS KR laser diffraction particle sizer. Table S1 in Supporting Information S1 provides the numerical data included in the endmember mixing model for river catchment ages (million years).

## Acknowledgments

EJP is supported by the NERC GW4+ Doctoral Training Partnership from the Natural Environment Research Council, grant number NE/L002434/1. This work was partly supported by the Research Council of Norway through its Centers of Excellence funding scheme, SFF Centre for Early Sapiens behaviour (SapienCE), project number 262618. We thank Lindsey Owen, Tony Oldroyd, CELTIC lab technicians, and Marc Alban-Millet for analytical support.

## References

- Åberg, G., Jacks, G., & Joseph Hamilton, P. (1989). Weathering rates and  $^{87}\text{Sr}/^{86}\text{Sr}$  ratios: An isotopic approach. *Journal of Hydrology*, 109(1–2), 65–78. [https://doi.org/10.1016/0022-1694\(89\)90007-3](https://doi.org/10.1016/0022-1694(89)90007-3)
- Bayon, G., Burton, K. W., Soulet, G., Vigier, N., Dennielou, B., Etoubleau, J., et al. (2009). Hf and Nd isotopes in marine sediments: Constraints on global silicate weathering. *Earth and Planetary Science Letters*, 277(3–4), 318–326. <https://doi.org/10.1016/j.epsl.2008.10.028>
- Bayon, G., German, C. R., Boella, R. M., Milton, J. A., Taylor, R. N., & Nesbitt, R. W. (2002). An improved method for extracting marine sediment fractions and its application to Sr and Nd isotopic analysis. *Chemical Geology*, 187(3–4), 179–199. [https://doi.org/10.1016/S0009-2541\(01\)00416-8](https://doi.org/10.1016/S0009-2541(01)00416-8)
- Bayon, G., Toucanne, S., Skonieczny, C., André, L., Bermell, S., Cheron, S., et al. (2015). Rare earth elements and neodymium isotopes in world river sediments revisited. *Geochimica et Cosmochimica Acta*, 170, 17–38. <https://doi.org/10.1016/j.gca.2015.08.001>
- Beny, F., Bout-Roumazeilles, V., Davies, G. R., Waelbroeck, C., Bory, A., Tribouillard, N., et al. (2020). Radiogenic isotopic and clay mineralogical signatures of Terrigenous particles as water-mass tracers: New insights into South Atlantic deep circulation during the last termination. *Quaternary Science Reviews*, 228, 106089. <https://doi.org/10.1016/j.quascirev.2019.106089>
- Birkett, C. K., Hill, T., Zuma, K. D., & Everson, T. M. (2016). Bringing rain to the land: Rainfall simulation as a participatory teaching aid to understanding erosion. *Journal of Environmental Protection*, 07(10), 1305–1316. <https://doi.org/10.4236/jep.2016.71014>
- Biscaye, P. E. (1965). Mineralogy and sedimentation of recent deep-sea clay in the Atlantic Ocean and adjacent seas and oceans. *Geological Society of America Bulletin*, 76(July), 803–832. [https://doi.org/10.1130/0016-7606\(1965\)76\[803:masord\]2.0.co;2](https://doi.org/10.1130/0016-7606(1965)76[803:masord]2.0.co;2)
- Biscaye, P. E., & Dasch, E. J. (1971). The rubidium, strontium, strontium-isotope system in deep-sea sediments: Argentine basin. *Journal of Geophysical Research*, 76(21), 5087–5096. <https://doi.org/10.1029/jc076i021p05087>
- Blanchet, C. L., Osborne, A. H., Tjallingii, R., Ehrmann, W., Friedrich, T., Timmermann, A., et al. (2021). Drivers of river reactivation in North Africa during the last glacial cycle. *Nature Geoscience*, 14(2), 97–103. <https://doi.org/10.1038/s41561-020-00671-3>
- Blaser, P., Lippold, J., Gutjahr, M., Frank, N., Link, J. M., & Frank, M. (2016). Extracting foraminiferal seawater Nd isotope signatures from bulk deep sea sediment by chemical leaching. *Chemical Geology*, 439, 189–204. <https://doi.org/10.1016/j.chemgeo.2016.06.024>
- Blum, J. D., & Erel, Y. (1997). Rb-Sr isotope systematics of a granitic soil chronosequence: The importance of biotite weathering. *Geochimica et Cosmochimica Acta*, 61(15), 3193–3204. [https://doi.org/10.1016/S0016-7037\(97\)00148-8](https://doi.org/10.1016/S0016-7037(97)00148-8)
- Blum, J. D., & Erel, Y. (2003). Radiogenic isotopes in weathering and hydrology. *Treatise on Geochemistry*, 5(9), 365–392. <https://doi.org/10.1016/B0-08-043751-6/05082-9>
- Blum, J. D., Erel, Y., & Brown, K. (1993).  $^{87}\text{Sr}/^{86}\text{Sr}$  ratios of Sierra Nevada stream waters: Implications for relative mineral weathering rates. *Geochimica et Cosmochimica Acta*, 57(21–22), 5019–5025. [https://doi.org/10.1016/S0016-7037\(05\)80014-6](https://doi.org/10.1016/S0016-7037(05)80014-6)
- Camberlin, P., Janicot, S., & Pocard, I. (2001). Seasonality and atmospheric dynamics of the teleconnection between African rainfall and tropical sea surface temperature: Atlantic vs ENSO. *International Journal of Climatology*, 21, 973–1005. <https://doi.org/10.1002/2016JD025277>
- Capo, R. C., Stewart, B. W., & Chadwick, O. A. (1998). Strontium isotopes as tracers of ecosystem processes: Theory and methods. *Geoderma*, 82(1–3), 197–225. [https://doi.org/10.1016/S0016-7061\(97\)00102-X](https://doi.org/10.1016/S0016-7061(97)00102-X)
- Carter, S. C., Griffith, E. M., Clift, P. D., Scher, H. D., & Dellapenna, T. M. (2020). Clay-fraction strontium and neodymium isotopes in the Indus fan: Implications for sediment transport and provenance. *Geological Magazine*, 157(6), 1–16. <https://doi.org/10.1017/s0016756820000394>
- Castañeda, I. S., Caley, T., Dupont, L., Kim, J. H., Malaizé, B., & Schouten, S. (2016). Middle to Late Pleistocene vegetation and climate change in subtropical Southern East Africa. *Earth and Planetary Science Letters*, 450, 306–316. <https://doi.org/10.1016/j.epsl.2016.06.049>
- Catuneanu, O., Wopfner, H., Eriksson, P. G., Cairncross, B., Rubidge, B. S., Smith, R. M. H., & Hancox, P. J. (2005). The Karoo basins of South-central Africa. *Journal of African Earth Sciences*, 43(1–3), 211–253. <https://doi.org/10.1016/j.jafrearsci.2005.07.007>
- Cawthra, H. C., Cowling, R. M., Andò, S., & Marean, C. W. (2020). Geological and soil maps of the Palaeo-Agulhas plain for the last glacial maximum. *Quaternary Science Reviews*, 235, 105858. <https://doi.org/10.1016/j.quascirev.2019.07.040>
- Chamley, H. (1989). Clay sedimentology. *Clay Sedimentology*. <https://doi.org/10.1007/978-3-642-85916-8>



- Charlier, B. L. A., Ginibre, C., Morgan, D., Nowell, G. M., Pearson, D. G., Davidson, J. P., & Ottley, C. J. (2006). Methods for the microsampling and high-precision analysis of strontium and rubidium isotopes at single crystal scale for petrological and geochronological applications. *Chemical Geology*, 232(3–4), 114–133. <https://doi.org/10.1016/j.chemgeo.2006.02.015>
- Chase, B. M., & Meadows, M. E. (2007). Late Quaternary dynamics of Southern Africa's winter rainfall zone. *Earth-Science Reviews*, 84(3–4), 103–138. <https://doi.org/10.1016/j.earscirev.2007.06.002>
- Chen, J., Liu, P., Sun, D., Zhang, D., Miao, B., & Chen, J. (2020). Riverine sediment geochemistry as provenance fingerprints along the eastern coast of China: Constraint, approach, and application. *Minerals*, 10(1), 29. <https://doi.org/10.3390/min10010029>
- Compton, J. S. (2004). The rocks and Mountains of Cape Town. *Juta and Company Ltd*, 2004, 9781919930701.
- Compton, J. S. (2011). Pleistocene sea-level fluctuations and human evolution on the southern coastal plain of South Africa. *Quaternary Science Reviews*, 30(5–6), 506–527. <https://doi.org/10.1016/j.quascirev.2010.12.012>
- Compton, J. S., & Maake, L. (2007). Source of the suspended load of the upper Orange River, South Africa. *South African Journal of Geology*, 110(2–3), 339–348. <https://doi.org/10.2113/gssaajg.110.2-3.339>
- Compton, J. S., & Wiltshire, J. G. (2009). Terrigenous sediment export from the Western Margin of South Africa on glacial to interglacial cycles. *Marine Geology*, 266(1–4), 212–222. <https://doi.org/10.1016/j.margeo.2009.08.013>
- Dasch, E. J. (1969). Strontium isotopes in weathering profiles, deep-sea sediments, and sedimentary rocks. *Geochimica et Cosmochimica Acta*, 33(12), 1521–1552. [https://doi.org/10.1016/0016-7037\(69\)90153-7](https://doi.org/10.1016/0016-7037(69)90153-7)
- Dellinger, M., Gaillardet, J., Bouchez, J., Calmels, D., Louvat, P., Dosseto, A., et al. (2015). Riverine Li isotope fractionation in the Amazon River basin controlled by the weathering regimes. *Geochimica et Cosmochimica Acta*, 164, 71–93. <https://doi.org/10.1016/j.gca.2015.04.042>
- Derry, L. A., & France-Lanord, C. (1996). EPSL Neogene Himalayan weathering history and river  $^{87}\text{Sr}/^{86}\text{Sr}$ : Impact on the marine Sr record Pli SOO12-821X. *Earth and Planetary Science Letters*, 142(1–2), 59–74. [https://doi.org/10.1016/0012-821X\(96\)00091-x](https://doi.org/10.1016/0012-821X(96)00091-x)
- Dinis, P. A., Garzanti, E., Hahn, A., Vermeesch, P., & Cabral-Pinto, M. (2020). Weathering indices as climate proxies: A step forward based on Congo and SW African river muds. *Earth-Science Reviews*, 201(November 2019), 103039. <https://doi.org/10.1016/j.earscirev.2019.103039>
- Dupont, L. M., Caley, T., Kim, J. H., Castañeda, I., Malaizé, B., & Giraudeau, J. (2011). Glacial-interglacial vegetation dynamics in South Eastern Africa coupled to sea surface temperature variations in the Western Indian Ocean. *Climate of the Past*, 7(4), 1209–1224. <https://doi.org/10.5194/cp-7-1209-2011>
- Dupont, L. M., Zhao, X., Charles, C., Faith, J. T., & Braun, D. R. (2021). Continuous vegetation record of the Greater Cape Floristic Region (South Africa) covering the past 300 thousand years (IODP U1479) (pp. 1–32).
- Eglington, B. M., & Armstrong, R. A. (2004). The Kaapvaal Craton and adjacent Orogens, southern Africa: A geochronological database and overview of the geological development of the craton. *South African Journal of Geology*, 107(1–2), 13–32. <https://doi.org/10.2113/107.1-2.13>
- Fagel, N. (2007). Proxies in late Cenozoic paleoceanography. *Developments in Marine Geology*, 1(07), 139–184. [https://doi.org/10.1016/S1572-5480\(07\)01009-3](https://doi.org/10.1016/S1572-5480(07)01009-3)
- Fagel, N., Hillaire-Marcel, C., Humblet, M., Brasseur, R., Weis, D., & Stevenson, R. (2004). Nd and Pb isotope signatures of the clay-size fraction of Labrador Sea sediments during the Holocene: Implications for the inception of the modern deep circulation pattern. *Paleoceanography*, 19(3). <https://doi.org/10.1029/2003PA000993>
- Feng, J. L., Zhu, L. P., Zhen, X. L., & Hu, Z. G. (2009). Grain size effect on Sr and Nd isotopic compositions in Eolian dust: Implications for tracing dust provenance and Nd model age. *Geochemical Journal*, 43(2), 123–131. <https://doi.org/10.2343/geochemj.1.0007>
- Flemming, B. W. (1981). Factors controlling shelf sediment dispersal along the Southeast African continental margin. *Marine Geology*, 42(1–4), 259–277. [https://doi.org/10.1016/0025-3227\(81\)90166-3](https://doi.org/10.1016/0025-3227(81)90166-3)
- Font, L., Nowell, G. M., Graham Pearson, D., Ottley, C. J., & Willis, S. G. (2007). Sr isotope analysis of bird feathers by TIMS: A tool to trace bird migration paths and breeding sites. *Journal of Analytical Atomic Spectrometry*, 22(5), 513–522. <https://doi.org/10.1039/B616328A>
- Franzese, A. M., Hemming, S. R., Goldstein, S. L., & Anderson, R. F. (2006). Reduced Agulhas Leakage during the last glacial maximum inferred from an integrated provenance and flux study. *Earth and Planetary Science Letters*, 250(1–2), 72–88. <https://doi.org/10.1016/j.epsl.2006.07.002>
- Frenken, Faurès, & Division (1997). *Irrigation potential in Africa: A basin approach*. Food and Agriculture Organization of the United Nations.
- Garzanti, E., Padoan, M., Peruta, L., Setti, M., & Villa, I. M. (2013). Weathering geochemistry and Sr-Nd fingerprints of equatorial upper Nile and Congo muds. *Geochemistry, Geophysics, Geosystems*, 14(2), 292–316. <https://doi.org/10.1002/ggge.20060>
- Garzanti, E., Padoan, M., Setti, M., López-Galindo, A., & Villa, I. M. (2014). Provenance versus weathering control on the composition of tropical river mud (Southern Africa). *Chemical Geology*, 366, 61–74. <https://doi.org/10.1016/j.chemgeo.2013.12.016>
- Goddard, L., & Graham, N. E. (1999). Importance of the Indian Ocean for simulating rainfall anomalies over Eastern and Southern Africa. *Journal of Geophysical Research*, 104(16), 19099–19116. [https://doi.org/10.1007/0-387-25098-0\\_13](https://doi.org/10.1007/0-387-25098-0_13)
- Goldstein, S. L., Nions, R. K. O., Hamilton, P. J., O'Nions, R. K., & Hamilton, P. J. (1984). A Sm-Nd isotopic study of atmospheric dusts and particulates from major river systems. *Earth and Planetary Science Letters*, 70(2), 221–236. [https://doi.org/10.1016/0012-821X\(84\)90007-4](https://doi.org/10.1016/0012-821X(84)90007-4)
- Granet, M., Chabaux, F., Stille, P., Dosseto, A., France-Lanord, C., & Blaes, E. (2010). U-series disequilibria in suspended river sediments and implication for sediment transfer time in alluvial plains: The case of the Himalayan rivers. *Geochimica et Cosmochimica Acta*, 74(10), 2851–2865. <https://doi.org/10.1016/j.gca.2010.02.016>
- Green, A. (2009). Sediment dynamics on the narrow, canyon-incised and current-swept shelf of the Northern KwaZulu-Natal continental shelf, South Africa. *Geo-Marine Letters*, 29(4), 201–219. <https://doi.org/10.1007/s00367-009-0135-9>
- Grousset, F. E., & Biscaye, P. E. (2005). Tracing dust sources and transport patterns using Sr, Nd and Pb isotopes. *Chemical Geology*, 222(3–4), 149–167. <https://doi.org/10.1016/j.chemgeo.2005.05.006>
- Grousset, F. E., Biscaye, P. E., Zindler, A., Prospero, J., & Chester, R. (1988). Neodymium isotopes as tracers in marine sediments and aerosols: North Atlantic. *Earth and Planetary Science Letters*, 87(4), 367–378. [https://doi.org/10.1016/0012-821X\(88\)90001-5](https://doi.org/10.1016/0012-821X(88)90001-5)
- Grousset, F. E., Parra, M., Bory, A., Martinez, P., Bertrand, P., Shimmield, G., & Ellam, R. M. (1998). Saharan wind regimes traced by the Sr-Nd isotopic composition of subtropical Atlantic sediments: Last Glacial Maximum vs today. *Quaternary Science Reviews*, 17(4–5), 395–409. [https://doi.org/10.1016/S0277-3791\(97\)00048-6](https://doi.org/10.1016/S0277-3791(97)00048-6)
- Grousset, F. E., Rognon, P., Coudé-Gaussen, G., & Pédemay, P. (1992). Origins of peri-Saharan dust deposits traced by their Nd and Sr isotopic composition. *Palaeogeography, Palaeoclimatology, Palaeoecology*, 93(3–4), 203–212. [https://doi.org/10.1016/0031-0182\(92\)90097-0](https://doi.org/10.1016/0031-0182(92)90097-0)
- Gutjahr, M., Frank, M., Stirling, C. H., Klemm, V., van de Fliedert, T., & Halliday, A. N. (2007). Reliable extraction of a deepwater trace metal isotope signal from Fe-Mn oxyhydroxide coatings of marine sediments. *Chemical Geology*, 242(3–4), 351–370. <https://doi.org/10.1016/j.chemgeo.2007.03.021>
- Hahn, A., Compton, J. S., Meyer-Jacob, C., Kirsten, K. L., Lucassen, F., Pérez Mayo, M., et al. (2016). Holocene paleo-climatic record from the South African Namaqualand Mudbelt: A source to sink approach. *Quaternary International*, 404, 121–135. <https://doi.org/10.1016/j.quaint.2015.10.017>

- Hahn, A., Miller, C., Andó, S., Bouimetarhan, I., Cawthra, H. C., Garzanti, E., et al. (2018). The provenance of terrigenous components in marine sediments along the east coast of Southern Africa. *Geochemistry, Geophysics, Geosystems*, 19(7), 1946–1962. <https://doi.org/10.1029/2017GC007228>
- Hahn, A., Schefuß, E., Andó, S., Cawthra, H. C., Frenzel, P., Kugel, M., et al. (2017). Southern Hemisphere anticyclonic circulation drives oceanic and climatic conditions in late Holocene Southernmost Africa. *Climate of the Past*, 13(6), 649–665. <https://doi.org/10.5194/cp-13-649-2017>
- Harris, C., Compton, J. S., & Bevington, S. A. (1999). Oxygen and hydrogen isotope composition of kaolinite deposits, Cape Peninsula, South Africa: Low-temperature, meteoric origin. *Economic Geology*, 94(8), 1353–1366. <https://doi.org/10.2113/gsecongeo.94.8.1353>
- Harris, C. R., Millman, K. J., van der Walt, S. J., Gommers, R., Virtanen, P., Cournapeau, D., et al. (2020). Array programming with NumPy. *Nature*, 585(7825), 357–362. <https://doi.org/10.1038/s41586-020-2649-2>
- He, J., Garzanti, E., Dinis, P., Yang, S., & Wang, H. (2020). Provenance versus weathering control on sediment composition in tropical monsoonal climate (South China)—I. Geochemistry and clay mineralogy. *Chemical Geology*, 558(September), 119860. <https://doi.org/10.1016/j.chemgeo.2020.119860>
- Herbert, C. T. (2009). *Holocene sediment dynamics on the western margin of South Africa* (Ph.D Thesis) (p. 277). University of Cape Town.
- Hjulström, F. (1955). Transportation of detritus by moving Water I. In P. D. Trask (Ed.), *Recent Marine sediments*. SEPM Society for Sedimentary Geology. <https://doi.org/10.2110/pec.55.04.0005>
- Hoffman, T. M., & Todd, S. (2000). A national review of land degradation in South Africa: The influence of biophysical and socio-economic factors. *Journal of Southern African Studies*, 26(4), 743–758. <https://doi.org/10.1080/713683611>
- Hu, B., Li, G., Li, J., Bi, J., Zhao, J., & Bu, R. (2012). Provenance and climate change inferred from Sr-Nd-Pb isotopes of late Quaternary sediments in the Huanghe (Yellow River) Delta, China. *Quaternary Research (United States)*, 78(3), 561–571. <https://doi.org/10.1016/j.yqres.2012.07.005>
- Jacobsen, S. B., & Wasserburg, G. J. (1980). Sm-Nd Isotopic systematics of chondrites and achondrites. *Division of Geol. Plan. Sci.*, 346(358), 307–308.
- Jelsma, H. A., & Dirks, P. H. G. M. (2002). Neoarchaean tectonic evolution of the Zimbabwe Craton. *Geological Society—Special Publications*, 199(1), 183–211. <https://doi.org/10.1144/GSL.SP.2002.199.01.10>
- Jewell, A. M., Cooper, M. J., Milton, J. A., James, R. H., Crocker, A. J., & Wilson, P. A. (2022). Chemical isolation and isotopic analysis of Terrigenous sediments with emphasis on effective removal of Contam-Inating Marine phases including barite. *Chemical Geology*, 589(July 2021), 120673. <https://doi.org/10.1016/j.chemgeo.2021.120673>
- Jewell, A. M., Drake, N., Crocker, A. J., Bakker, N. L., Kunkelova, T., Bristow, C. S., et al. (2021). Three North African dust source areas and their geochemical fingerprint. *Earth and Planetary Science Letters*, 554, 116645. <https://doi.org/10.1016/j.epsl.2020.116645>
- Jochum, K. P., Nohl, U., Herwig, K., Lammel, E., Stoll, B., & Hofmann, A. W. (2005). GeoReM: A new geochemical database for reference materials and isotopic standards. *Geostandards and Geoanalytical Research*, 29(3), 333–338. <https://doi.org/10.1111/j.1751-908X.2005.tb00904.x>
- Jonell, T. N., Carter, A., Böning, P., Pahnke, K., & Clift, P. D. (2017). Climatic and glacial impact on erosion patterns and sediment provenance in the Himalayan rain shadow, Zaskar River, NW India. *Bulletin of the Geological Society of America*, 129(7–8), 820–836. <https://doi.org/10.1130/B31573.1>
- Jonell, T. N., Li, Y., Blusztajn, J., Giosan, L., & Clift, P. D. (2018). Signal or noise? Isolating grain size effects on Nd and Sr isotope variability in Indus delta sediment provenance. *Chemical Geology*, 485(February), 56–73. <https://doi.org/10.1016/j.chemgeo.2018.03.036>
- Jung, S. J. A., Davies, G. R., Ganssen, G. M., & Kroon, D. (2004). Stepwise Holocene aridification in NE Africa deduced from dust-borne radiogenic isotope records. *Earth and Planetary Science Letters*, 221(1–4), 27–37. [https://doi.org/10.1016/S0012-821X\(04\)00095-0](https://doi.org/10.1016/S0012-821X(04)00095-0)
- Kuhn, G., & Diekmann, B. (2002). Late Quaternary variability of ocean circulation in the southeastern South Atlantic inferred from the terrigenous sediment record of a drift deposit in the Southern Cape Basin (ODP Site 1089). *Palaeogeography, Palaeoclimatology, Palaeoecology*, 182(3–4), 287–303. [https://doi.org/10.1016/S0031-0182\(01\)00500-4](https://doi.org/10.1016/S0031-0182(01)00500-4)
- Kunkelova, T., Crocker, A. J., Jewell, A. M., Breeze, P. S., Drake, N. A., Cooper, M. J., et al. (2022). Dust sources in Westernmost Asia have a different geochemical fingerprint to those in the Sahara. *Quaternary Science Reviews*, 294, 107717. <https://doi.org/10.1016/j.quascirev.2022.107717>
- Lambart, S., Koornneef, J. M., Millet, M. A., Davies, G. R., Cook, M., & Lissenberg, C. J. (2019). Highly heterogeneous depleted mantle recorded in the lower oceanic crust. *Nature Geoscience*, 12(6), 482–486. <https://doi.org/10.1038/s41561-019-0368-9>
- Lehner, B., & Grill, G. (2013). Global river hydrography and network routing: Baseline data and new approaches to study the world's large river systems. *Hydrological Processes*, 27(15), 2171–2186. <https://doi.org/10.1002/hyp.9740>
- Le Roux, J. J. (2007). Monitoring soil erosion in South Africa at a regional scale for deposition. *South African Journal of Science*, 103(August), 329–335.
- Luttinen, A. V., Rämö, O. T., & Huhma, H. (1998). Neodymium and strontium isotopic and trace element composition of a Mesozoic CFB suite from Dronning Maud Land, Antarctica: Implications for lithosphere and asthenosphere contributions to Karoo magmatism. *Geochimica et Cosmochimica Acta*, 62, 2701–2714. [https://doi.org/10.1016/S0016-7037\(98\)00184-7](https://doi.org/10.1016/S0016-7037(98)00184-7)
- Maccali, J., Hillaire-Marcel, C., & Not, C. (2018). Radiogenic isotope (Nd, Pb, Sr) signatures of surface and sea ice-transported sediments from the Arctic Ocean under the present interglacial conditions. *Polar Research*, 37(1), 1442982. <https://doi.org/10.1080/17518369.2018.1442982>
- Maitre, D. L., Colvin, C., & Maherry, A. (2009). Water resources in the Klein Karoo: The challenge of sustainable development in a water-scarce area. *South African Journal of Science*, 105(1–2), 39–48. <https://doi.org/10.1590/s0038-23532009000100019>
- Makhubela, T. V., Kramers, J., Konyana, S., Van Niekerk, H., & Winkler, S. (2021). Erosion rates and weathering timescales in the Eastern Great Escarpment, South Africa. *Chemical Geology*, 580, 120368. <https://doi.org/10.1016/j.chemgeo.2021.120368>
- Mason, S. J. (1995). Sea-Surface temperature — South African rainfall associations, 1910–1989. *International Journal of Climatology*, 15(2), 119–135. <https://doi.org/10.1002/JOC.3370150202>
- Mccoy-west, A. J., Millet, M., & Burton, K. W. (2017). The neodymium stable isotope composition of the silicate Earth and chondrites. *Earth and Planetary Science Letters*, 480, 121–132. <https://doi.org/10.1016/j.epsl.2017.10.004>
- Meyer, I., Davies, G. R., & Stuut, J. B. W. (2011). Grain size control on Sr-Nd isotope provenance studies and impact on paleoclimate reconstructions: An example from deep-sea sediments offshore NW Africa. *Geochemistry, Geophysics, Geosystems*, 12(3), 1–14. <https://doi.org/10.1029/2010GC003355>
- Moore, A., Blenkinsop, T., & Cotterill, F. (2009). Southern African topography and erosion history: Plumes or plate tectonics? *Terra Nova*, 21(4), 310–315. <https://doi.org/10.1111/j.1365-3121.2009.00887.x>
- Nash, D. J. (2017). Changes in precipitation over southern Africa during recent centuries.
- Neumann, E. R., Svensen, H., Galerne, C. Y., & Planke, S. (2011). Multistage evolution of dolerites in the Karoo large igneous province, Central South Africa. *Journal of Petrology*, 52(5), 959–984. <https://doi.org/10.1093/petrology/egr011>

- Paterson, G. A., & Heslop, D. (2015). New methods for unmixing sediment grain size data. *Geochemistry, Geophysics, Geosystems*, 16(12), 4494–4506. <https://doi.org/10.1002/2015GC006070>
- Petschick, R., Kuhn, G., & Ginge, F. (1996). Clay mineral distribution in surface sediments of the South Atlantic: Sources, transport, and relation to oceanography. *Marine Geology*, 130(3–4), 203–229. [https://doi.org/10.1016/0025-3227\(95\)00148-4](https://doi.org/10.1016/0025-3227(95)00148-4)
- Pryor, E. J. (2024). Data set: Geochemical—Mineralogical constraints on the provenance of sediment supplied from South African river catchments draining into the Southwestern Indian Ocean. <https://doi.org/10.5281/zenodo.13608833>
- Pryor, E. J., Tangunan, D., van der Lubbe, H. J. L., Simon, M. H., & Hall, I. R. (2024). Recommended centrifuge method: Specific grain size separation in the <63 µm fraction of marine sediments. *MethodsX*, 12, 102718. <https://doi.org/10.1016/j.mex.2024.102718>
- Reason, C. J. C., & Mulenga, H. (1999). Relationships between South African rainfall and SST anomalies in the Southwest Indian Ocean. *International Journal of Climatology*, 19(15), 1651–1673. [https://doi.org/10.1002/\(SICI\)1097-0088\(199912\)19:15<1651::AID-JOC439>3.0.CO;2-U](https://doi.org/10.1002/(SICI)1097-0088(199912)19:15<1651::AID-JOC439>3.0.CO;2-U)
- Riley, T. R., Curtis, M. L., Leat, P. T., Watkeys, M. K., Duncan, R. A., Millar, I. L., & Owens, W. H. (2005). Overlap of Karoo and Ferrar magma types in KwaZulu-Natal, South Africa. *Journal of Petrology*, 47(3), 541–566. <https://doi.org/10.1093/petrology/egi085>
- Rooseboom, A., & Annandale, G. W. (1981). Techniques applied in determining sediment loads in South African rivers. Erosion and Sediment Transport Measurement. In *Proc. Florence symposium, June 1981* (Vol. 133, pp. 219–224). International Association of Hydrological Sciences, IAHS-AISH Publication 133.
- Rooseboom, A., Verster, E., Zietsman, H. L., & Lotriet, H. H. (1992). The development of the new sediment yield map of Southern Africa. *Water Research Commission Report*, 297(2), 92.
- Scorner, J., Faillace, K. E., Hildred, A., Nederbragt, A. J., Andersen, M. B., Millet, M. A., et al. (2021). Diversity aboard a Tudor warship: Investigating the origins of the Mary Rose crew using multi-isotope analysis. *Royal Society Open Science*, 8(5). <https://doi.org/10.1098/rsos.202106>
- Seutloali, K. E., Beckedahl, H. R., Dube, T., & Sibanda, M. (2016). An assessment of gully erosion along major armoured roads in South-eastern region of South Africa: A remote sensing and GIS approach. *Geocarto International*, 31(2), 225–239. <https://doi.org/10.1080/10106049.2015.1047412>
- Simon, M. H., Babin, D. P., Goldstein, S. L., Cai, M. Y., Liu, T., Han, X., et al. (2020a). Development of a protocol to obtain the composition of terrigenous detritus in marine sediments -a pilot study from International Ocean Discovery Program Expedition 361. *Chemical Geology*, 535(April 2019), 119449. <https://doi.org/10.1016/j.chemgeo.2019.119449>
- Simon, M. H., Babin, D. P., Goldstein, S. L., Cai, M. Y., Liu, T., Han, X., et al. (2020b). Sequential extraction procedure to obtain the composition of terrigenous detritus in marine sediments. *MethodsX*, 7, 100888. <https://doi.org/10.1016/j.mex.2020.100888>
- Simon, M. H., Ziegler, M., Bosmans, J., Barker, S., Reason, C. J. C., & Hall, I. R. (2015). Eastern South African hydroclimate over the past 270,000 years. *Scientific Reports*, 5, 1–10. <https://doi.org/10.1038/srep18153>
- Stager, J. C., Ryves, D. B., Chase, B. M., & Pausata, F. S. R. (2011). Catastrophic drought in the Afro-Asian monsoon region during Heinrich event 1. *Science*, 331(6022), 1299–1302. <https://doi.org/10.1126/science.1198322>
- Stewart, B. A., Zhao, Y., Mitchell, P. J., Dewar, G., Gleason, J. D., & Blum, J. D. (2020). Ostrich eggshell bead strontium isotopes reveal persistent macroscale social networking across late Quaternary Southern Africa. *Proceedings of the National Academy of Sciences of the United States of America*, 117(12), 6453–6462. <https://doi.org/10.1073/pnas.1921037117>
- Strobel, P., Kasper, T., Frenzel, P., Schitteck, K., Quick, L. J., Meadows, M. E., et al. (2019). Late Quaternary palaeoenvironmental change in the year-round rainfall zone of South Africa derived from peat sediments from Vankervelsvlei. *Quaternary Science Reviews*, 218, 200–214. <https://doi.org/10.1016/j.quascirev.2019.06.014>
- Taljaard, S. (2003). Department of water affairs and forestry Breede river basin study intermediate determination of resource directed measures.
- Thieblemont, D. (2017). An updated geological map of Africa at 1/10 000 000 scale (pp. 1–2).
- Tierney, J. E., Smerdon, J. E., Anchukaitis, K. J., & Seager, R. (2013). Multidecadal variability in East African hydroclimate controlled by the Indian ocean. *Nature*, 493(7432), 389–392. <https://doi.org/10.1038/nature11785>
- van der Lubbe, J. H. J. L., Frank, M., Tjallingii, R., & Ralph, R. S. (2016). Neodymium isotope constraints on provenance, dispersal, and climate-driven supply of Zambezi sediments along the Mozambique Margin during the past ~45,000 years. *Geochemistry, Geophysics, Geosystems*, 18(1–2), 1–10. <https://doi.org/10.1002/2014GC005684>
- van der Lubbe, J. H. J. L., Tjallingii, R., Prins, M. A., Brummer, G. J. A., Jung, S. J. A., Kroon, D., & Schneider, R. R. (2014). Sedimentation patterns off the Zambezi River over the last 20,000 years. *Marine Geology*, 355, 189–201. <https://doi.org/10.1016/j.margeo.2014.05.012>
- van der Merwe, C. R., & Weber, H. W. (1963). Clay minerals of South African soils. *South African Journal of Agricultural Science*, 6, 411–454.
- Walker, N. D. (1990). Links between South African summer rainfall and temperature variability of the Agulhas and Benguela current system. *Journal of Geophysical Research*, 95(C3), 3297–3319. <https://doi.org/10.1029/jc095ic03p03297>
- Walling, D. E. (1984). The sediment yields of African rivers. In *Challenges in African Hydrology & water resources, Proc. Harare Symp., (Harare, Zimbabwe: July. 1984)*. D.E. Walling; S.S.D. 144.
- Walter, H. J., Hegner, E., Diekmann, B., Kuhn, G., & Rutgers Van Der Loeff, M. M. (2000). Provenance and transport of terrigenous sediment in the South Atlantic Ocean and their relations to glacial and interglacial cycles: Nd and Sr isotopic evidence. *Geochimica et Cosmochimica Acta*, 64(22), 3813–3827. [https://doi.org/10.1016/S0016-7037\(00\)00476-2](https://doi.org/10.1016/S0016-7037(00)00476-2)
- Weldeab, S., Stuut, J. B. W., Schneider, R. R., & Siebel, W. (2013). Holocene climate variability in the winter rainfall zone of South Africa. *Climate of the Past*, 9(5), 2347–2364. <https://doi.org/10.5194/cp-9-2347-2013>
- Ziegler, M., Simon, M. H., Hall, I. R., Barker, S., Stringer, C., Zahn, R., et al. (2013). Development of Middle Stone Age innovation linked to rapid climate change. *Nature Communications*, 4(May), 1905. <https://doi.org/10.1038/ncomms2897>